creative commons
COMMONS DEED

저작자표시-비영리-변경금지 2.0 대한민국

이용자는 아래의 조건을 따르는 경우에 한하여 자유롭게

- 이 저작물을 복제, 배포, 전송, 전시, 공연 및 방송할 수 있습니다.

다음과 같은 조건을 따라야 합니다:

저작자표시. 귀하는 원저작자를 표시하여야 합니다.

비영리. 귀하는 이 저작물을 영리 목적으로 이용할 수 없습니다.

변경금지. 귀하는 이 저작물을 개작, 변형 또는 가공할 수 없습니다.

- 귀하는, 이 저작물의 재이용이나 배포의 경우, 이 저작물에 적용된 이용허락조건을 명확하게 나타내어야 합니다.
- 저작권자로부터 별도의 허가를 받으면 이러한 조건들은 적용되지 않습니다.

저작권법에 따른 이용자의 권리는 위의 내용에 의하여 영향을 받지 않습니다.

이것은 이용허락규약(Legal Code)을 이해하기 쉽게 요약한 것입니다.

Disclaimer

dCollection

Master Thesis
석사 학위논문

A Low-Power Large-Dynamic-Range Time-Domain Interface Circuit for Resistive Gas Sensors

Bongsik Choi(최 봉 식 崔 鳳 植)

Department of
Information and Communication Engineering

DGIST

2017

A Low-Power Large-Dynamic-Range Time-Domain Interface Circuit for Resistive Gas Sensors Bongsik Choi 2017

Master Thesis
석사 학위논문

A Low-Power Large-Dynamic-Range Time-Domain Interface Circuit for Resistive Gas Sensors

Bongsik Choi(최 봉 식 崔 鳳 植)

Department of
Information and Communication Engineering

DGIST

2017

A Low-Power Large-Dynamic-Range Time-Domain Interface Circuit for Resistive Gas Sensors

Advisor: Professor Junghyup Lee

Co-Advisor: Professor Minkyu Je

by

Bongsik Choi

Department of Information and Communication Engineering

DGIST

A thesis submitted to the faculty of DGIST in partial fulfillment of the requirements for the degree of Master of Science in the Department of Information and Communication Engineering. The study was conducted in accordance with Code of Research Ethics[1)].

11. 11. 2016

Approved by

Professor Junghyup Lee (Signature)

(Advisor)

Professor Minkyu Je (Signature)

(Co-Advisor)

1) Declaration of Ethical Conduct in Research**:** I, as a graduate student of DGIST, hereby declare that I have not committed any acts that may damage the credibility of my research. These include, but are not limited to: falsification, thesis written by someone else, distortion of research findings or plagiarism. I affirm that my thesis contains honest conclusions based on my own careful research under the guidance of my thesis advisor.

A Low-Power Large-Dynamic-Range Time-Domain Interface Circuit for Resistive Gas Sensors

Bongsik Choi

Accepted in partial fulfillment of the requirements for the degree of Master of Science

11. 25. 2016

Head of Committee_____(인)

Prof. Junghyup Lee

Committee Member_____(인)

Prof. Minkyu Je

Committee Member_____(인)

Prof. Jae-Eun Jang

List of Contents

Abstract ……..iii

List of tables…….. v

List of figures……..vi

1. Introduction ……1

1.1 Motivation ……1

1.2 Gas sensing principle and resistance ranges……2

1.3 Resistance read-out methods ……...4

1.4 Proposed system and target specification……...7

1.5 Oscillator……...8

2. Background information: Frequency stability……12

2.1 Frequency domain……12

2.2 Time domain definitions……..14

2.3 Power-law noise models……15

2.4 Wiener-Khinchine theorem……16

2.5 Phase noise for designing oscillator……17

2.6 FOM……...17

3. Noise analysis……19

3.1 Input referred noise of inverter……...19

3.2 Noise contribution to phase noise……21

4. System structure & Operation principle……31

4.1 Structure block diagram……31

4.2 Details of each blocks……...32

4.3 Measurement operation and equations……37

4.4 Sensing resolution and Trade-off with measurement time……40

5. Schematic design and Layout……...41

5.1 Schematic design……42

5.2 Layout……...45

6. Simulation results……..48

6.1 Post layout simulation: Oscillator……...49

6.2 Post layout simulation: Programmable frequency converter and Frequency-to-Digital converter……..40

6.3 Size optimization of scalable inverter based oscillator……50

7. Conclusion & Future work……...51

8. Reference ……...53

MS/IC

201522023

최봉식. Bongsik Choi. A Low-Power Large-Dynamic-Range Time-Domain Interface Circuit for Resistive Gas Sensors. Department of Information and Communication Engineering. 54p. Advisors: Prof. Junghyup Lee. Co-Advisor: Prof. Minkyu Je

Abstract

This thesis is looks into a low-power large-dynamic-range time-domain interface circuit for resistive gas sensors. Recently, as the pollution of the air has attracted attention as a social problem, the regulation of the harmful gas of the government is becoming more and more subdivided. Gas sensor measurement systems are required to satisfy various gas sensor measurement ranges in order to satisfy the subdivided values according to the gas. One of the features of the thesis is that an inverter, which is able to change size, was applied to proceed with a low-power method and a signal was processed in time domain to possess wide measurement range. Another feature of the thesis is that by using swing-boosting method, this circuit has an advantage on noise characteristic. The size of the inverter is controlled by the size of the oscillator and the size of the inverter is controlled according to the operating frequency. The other feature is that it enables to adjust resolution in accordance with related purpose, using frequency divider. Besides, it enables to maintain optimal performance even in any resistance value through scalable method and frequency divider applied resolution adjustment. It is characterized by the ability to maintain optimal performance at any resistance value through resolution control using the size adjustment method and frequency divider. Hynix/Dongbu HiTek 0.18 process is applied through IDEC MPW. The circuit size is $0.35mm^2$, and power consumption is 150uW in 1V operation voltage.

Keywords: Resistance read-out system, Time domain, Scalable inverter, Swing-boost, PVT variation insensitive

요약문

저항식 가스센서 측정을 위한 저전력 넓은 동적범위를 갖는 시간 도메인 인터페이스 회로 설계

본 논문에서는 저전력으로 동작하는 넓은 측정 범위를 갖는 시간 도메인 저항식 가스센서 측정용 회로를 설계하였다. 최근 대기오염이 사회문제로 주목 받음에 따라 정부의 유해가스 규제가 세분화 되고 있다. 가스에 따라 세분화 된 수치를 만족시키기 위해서는 다양한 가스센서의 측정범위를 만족시키기 위한 가스센서 측정 시스템이 필요하다. 본 논문이 갖는 특징으로는 주파수를 만드는 발진기를 저전력 방식으로 동작하면서도 고성능 회로를 실현하기 위해 주파수에 따라 크기를 가변 할 수 있는 반전기를 사용하였고, swing-boosting 기법을 사용하여 노이즈에 강한 특성을 가지게 하였다. 발진기 내부의 크기 조절 반전기를 통해 동작 주파수에 따라 반전기의 크기를 조절을 통해 큰 크기의 반전기가 지터를 감소시켜 디지털 출력의 해상도를 높일 수 있도록 하였다. 또한 넓은 측정 범위를 갖기 위해 신호를 시간 도메인에서 처리하도록 하였고 목적에 따라 주파수 분주기를 통해 측정시간을 조절하여 해상도를 조절 할 수 있게 하였다. 크기 조절방식과 주파수 분주기를 사용한 해상도 조절을 통해 어떠한 저항 값에서도 최적의 성능을 유지 할 수 있는 특징이 있다. 설계는 IDEC MPW를 통한 하이닉스/동부하이텍 0.18μm 공정을 사용했으며, 회로의 크기는 0.35mm^2이고, 동작전압 1V에서 파워소모는 150uW이다.

핵심어: 크기 조절 반전기, 시간 도메인, 저항 측정용 회로, Swing-boost, PVT variation insensitive

List of Tables

Table 1: Indoor pollutant reason and recommended standard 1

Table 2: Measurable gas and resistivity change scale per sensor 4

Table 3: Target performance of proposed Resistance-to-Digital Converter 8

Table 4: Summary of noise models relationship 16

Table 5: Flicker noise and thermal noise of transistor, input referred noise of inverter 20

Table 6: Relationship between input referred noise of inverter and time error variance 24

Table 7: Relationship between time error variance and fractional frequency fluctuation PSD 27

Table 8: Relationship between fractional frequency fluctuation PSD and phase error PSD 29

Table 9: Relationship between Phase error PSD and Phase noise 30

Table 10: Comparison table about circuit performance 51

List of Figures

Figure 1: An object nature, which determines capacitance value 2

Figure 2: An object nature, which determines resistivity value 3

Figure 3: RV-AD type Single channel architecture 5

Figure 4: R-PD type Single channel architecture 6

Figure 5: Basic Relaxation oscillator circuit 8

Figure 6: The signal during charge and discharge cycle 10

Figure 7: ideal signal and noise signal 12

Figure 8: Noise signal to noise spectrum conversion 14

Figure 9: Relationship between Time domain and Frequency domain 15

Figure 10: Power-law model slopes of phase noise 16

Figure 11: Ideal oscillator and noisy oscillator output spectrum 17

Figure 12: The relationship between size of inverter and FOM 18

Figure 13: Small-signal model for input referred noise interpretation of the inverter. 19

Figure 14: Flow chart of overall noise interpretation. 21

Figure 15: Simplified RC oscillator 21

Figure 16: Voltage charging process of capacitor 22

Figure 17: Capacitor voltage in charging period, Relationship between voltage variance and time error variance 23

Figure 18: Time error variance and deviation 25

Figure 19: Averaged frequency deviation within time interval 25

Figure 20: System transfer function 26

Figure 21: Fractional frequency fluctuations to phase error derivation 29

Figure 22: Block diagram of the proposed resistance-to-digital converter 31

Figure 23: Schematic of the relaxation oscillator 32
Figure 24: Charge-Discharge phase and Swing-Boosted effect 34
Figure 25: Swing-Boosted effect in relaxation oscillator 34
Figure 26: the relationship between current source and time error 35
Figure 27: Programmable frequency divider 35
Figure 28: BCD-Thermometer Encoder 36
Figure 29: Free-running counter, registers, adder 37
Figure 30: RCD timing diagram in time domain 38
Figure 31: Timing diagram and Digital Output 39
Figure 32: Schematic of measurement oscillator 41
Figure 33: Schematic of reference oscillator 42
Figure 34: Scalable inverters 42
Figure 35: Unit size scalable inverter 43
Figure 36: Relationship between FOM and width, frequency and width 43
Figure 37: Relationship between FOM and length, frequency and length 44
Figure 38: Programmable frequency divider 44
Figure 39: Counter, registers, adder 45
Figure 40: Top merge layout of oscillators and digital block 45
Figure 41: Layout of measurement oscillator 46
Figure 42: Layout of reference oscillator 46
Figure 43: Digital block including PFD, Frequency-to-digital converter 47
Figure 44: Simulation results of schematic and PEX 48
Figure 45: Simulation result of digital block 49
Figure 46: Figure-of-merit according to resistance variation 50

1. Introduction

1.1 Motivation

People today spend 80~90% of their daily time indoor. Therefore, indoor air control is required as most of the daily time is spent indoor. Polluted indoor air (VOC) may cause sick house syndrome and it may be result of several environmental diseases (atopy, asthma etc.) [1]. The main cause of indoor air pollution includes pollutant entering indoor from outdoor, pollutant of construction material and indoor cooking etc.

Pollutant		**Cause** [1]	**Recommended standard** [2] [3]
Formaldehyde [2]		Plywood board, furniture, insulator, a cigarette smoke	0.08 ppm
Combustion gas [3]	CO	Stove, fuel burn, gas stove	11 ppm
	NO2		0.25 ppm
	SO2		0.38 ppm
VOCs	Toluene	A cigarette smoke, construction material, paint, heater (coal, oil burn)	0.07 ppm
	Xylene	Adhesive, paint	0.20 ppm
	Styrene	Adhesive, a plastic product	0.05 ppm

Table 1: Indoor pollutant reason and recommended standard

Recommended standard of several harmful gas is elaborated based on a national policy in purpose of air pollution control and protecting citizens from harmful gas [4]. Therefore, a system to measure concentration based on gas type has become more important than ever. Considering above effort, it is essential to develop read-out integrated circuit to apply to several gas systems in portable size, which notices potential danger in accordance with national recommended standard.

1.2 Gas sensing principles

1.2.1 Measurement principle of capacitive gas sensor

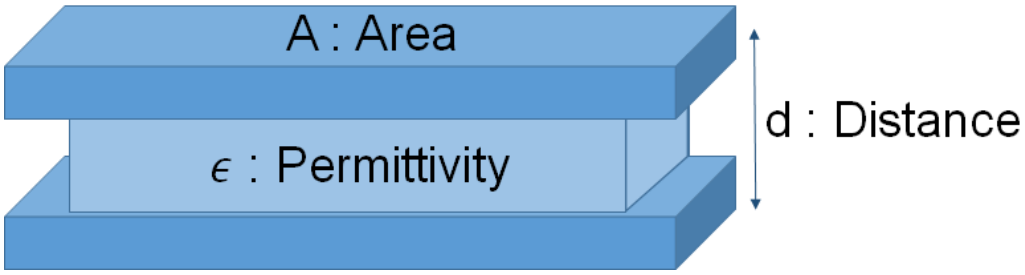

Figure 1: An object nature, which determines capacitance value

A formula for capacitance is shown below;

$$C = \frac{\varepsilon A}{d} \quad (\varepsilon = \varepsilon_0 \varepsilon_r) \tag{1}$$

Above shown **ε** stands for Permittivity and indicates accumulation degree of electric energy in electric field. It is original value based on an object. Permittivity (absolute permittivity) composes vacuum permittivity ε_0 and relative permittivity ε_r. Capacitance is determined based on size of two steel board, interval and middle dielectric object. Moreover, capacitance of the capacitive sensor is changed by changeable dielectric permittivity in accordance with gas concentration. Despite of the gas sensor in capacitive type, some permittivity is applied to high gas, such as ammonia, water vapor, and methane and most capacitive sensor are used for proximity, position, humidity, acceleration etc. instead of gas measurement [5].

1.2.2 Measurement principles of resistive gas sensor

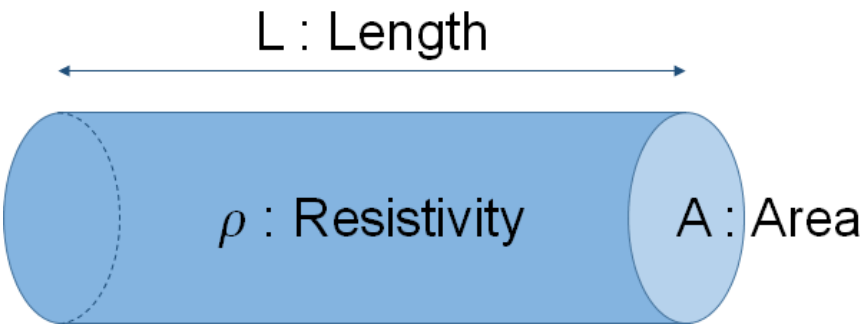

Figure 2: An object nature, which determines resistivity value

A formula for electrical resistivity of object is shown below;

$$R = \frac{\rho L}{A} \tag{2}$$

Above **ρ** stands for resistivity and is original value based on an object. **L** stands for the object length, **A** stands for cross sectional area of current object. Resistivity size is changed in the case of resistivity applied object length or area, electrical object nature change. Gas detective sensor part is called as chemiresistor and the object is varied in accordance with detectable gas type [6]. Gallium oxide is applied in the case of carbon monoxide measurement and tungsten oxide is applied in the case of carbon dioxide measurement. This method is called as metal oxide chemiresistor sensor. The sensor surface absorbable molecule number is changed based on gas concentration change in the sensors. The sensor resistivity changes in accordance with absorbance degree and consequently resistivity value is changed [5]. Most gas sensors in the market are resistive gas sensors, which applied above principles and their advantages are simple composition of sensor, robust operation and affordable manufacture cost. Therefore, resistive gas sensor is chosen under purpose of system circuit development, which is able to measure various gases.

Sensor	Manufacturer	Measurable gas	Measurement range	Resistivity change (initial resistivity)
MICS-4514 [7]	SGX Sensortech	CO	1~1000 ppm	70~150K ohm (70K ohm)
		NO_2	0.05~5 ppm	0.05~50M ohm (50K ohm)
AS-MLC [8]	AppliedSensor	CO	0.5~500 ppm	10~250K ohm (250K ohm)
AS-MLN [9]		NO_2	0.1~2 ppm	1~6M ohm (1M ohm)
AS-MLV [10]		VOCs	10~500 ppm	0.02~3M ohm (3M ohm)
GSBT11 [11]	Ogam	VOCs	0~350 ppm	12~20K ohm (12K ohm)

(VOCs: Alcohols, aldehydes, ketones, organic acids etc.)

Table 2: Measurable gas and resistivity change scale per sensor

Below shown table indicates resistivity change in accordance with gas sensor. Resistivity change scale is varied based on measurable gas and manufacturer. Even though standard resistivity and change scale are different, 5000 times difference exists between the smallest resistivity and the biggest resistivity from 10K to 50M scale. Resistivity of most gas sensor is changed within above scale. Therefore, from 10K to 50M scale has been set up to develop a gas sensor measurement system for common use.

1.3 Resistance read-out methods

Analog-digital conversion process is required for resistivity changeable gas sensor, digital signalization of resistivity change. Analog-digital conversion methods and their feature are shown below;

1.3.1 RV-ADC (Resistance-to-voltage using analog-to-digital conversion)

This method is used to convert digital value using changing voltage due to resistivity change in resistivity value change process based on the gas concentration of resistive gas sensor.

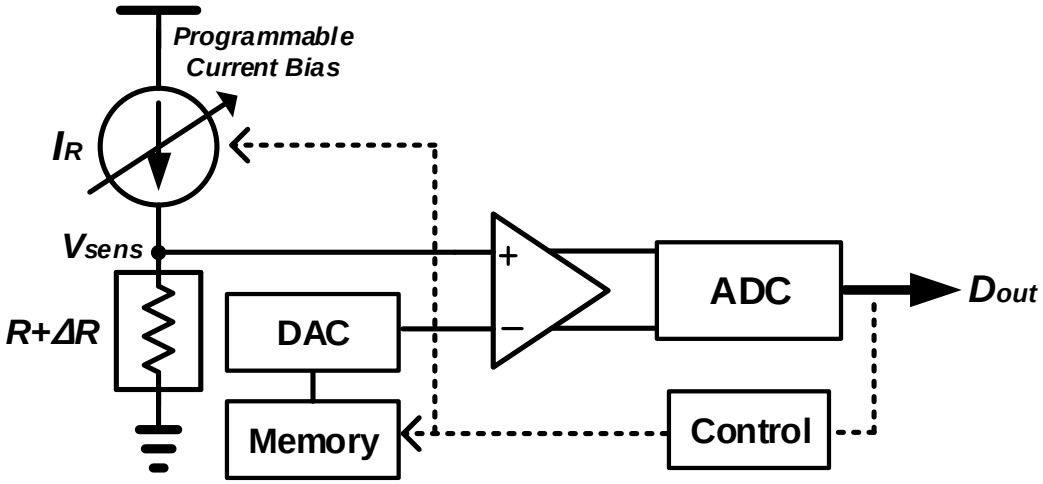

Figure 3: RV-AD type Single channel architecture

This paper, [12], is composed of programmable current bias, Memory register, 8bit DAC, ADC. Programmable current bias simply flows to sensor resistivity and makes sensor voltage. Baseline resistivity without gas is called R. $R + \Delta R$ is able to measure gas and changed resistivity. In this case, it saves baseline resistivity voltage in memory and measures pure resistivity change from $R + \Delta R$ voltage in gas insert. This thesis found the answer about smaller real resolution due to gas resistivity in comparison with baseline resistivity size of original readout circuit. Besides, nanoparticle coated chemiresistor arrays are applied to gas sensor for getting high sensitivity of special gas. This method is not suitable to the thesis purpose of making system, which is commonly used based on commercial sensors. In addition, measurable resistivity scale of 60K~10M does not meet the thesis goal of resistivity scale.

1.3.2 RP-FDC (Resistance-to-period using frequency-to-digital conversion)

In this method, frequency is changed as resistivity change from standard frequency and digital value is converted using frequency-digital converter based on resistive gas sensor concentration in resistivity value change process. Resolution is changed in accordance with measurement time, as it is not converted in voltage domain comparing with analog-digital converter.

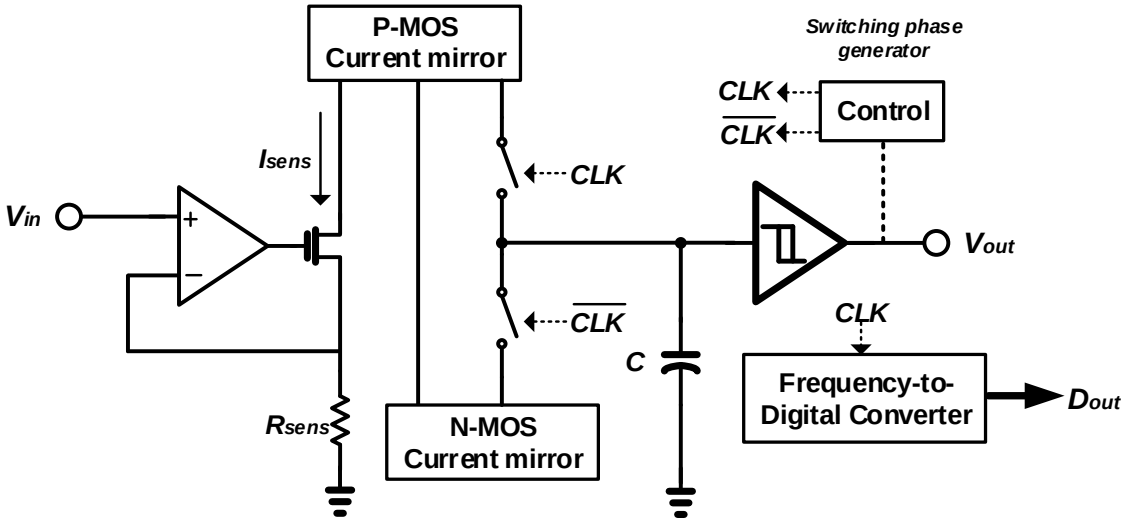

Figure 4: RP-FDC type Single channel architecture

These papers, [13] [14], are typical RP-FDC type readout circuit. I_{sens} is changed based on sensor resistivity and changed current is saved in capacitor. In the case of cycle, it is saved in capacitor and voltage is increased due to I_{sens} and phase is converted from charge to discharge once it is reached to high threshold voltage of Schmitt trigger. On the other hand, in the case of discharge, capacitor charged voltage is discharged as I_{sens} voltage. The discharge and discharge cycle make frequency and the frequency is converted to digital value through Frequency-to-digital converter. Introduced thesis is able to measure wide range resistivity of 300K to 300M using RP-FDC method is match with purpose and other parts of this thesis. However, high power consumption due to high operating voltage does not match with portable equipment integrated circuit design, which is based on low power operation.

1.3.3 RP-FDC selection reason

In the case of using RV-ADC as read-out system, which uses voltage domain to measure above-mentioned wide resistivity scale. Measurable minimum resistivity change is about 1.2K ohm in reading resistivity value of ADC, which possesses 12-bit resolution. In the case of GSTB11 sensor measurement from 0 to 350 ppm VOC gas concentration from 12K to 20K ohm, approximately 50ppm unit is measured per measurable 1.2K ohm of sensor resistivity. Besides, operating voltage of system shall be bigger than the size of gas sensor output voltage for digitalization of gas sensor output voltage. If operating voltage of system is smaller than gas sensor output, digitalized maximum value is indicated as saturation in system through ADC, even though real sensor output is

bigger that system voltage. In addition, it causes data loss. In the case of setting system supply voltage in sensor operating voltage, system circuit cannot be operated with low power.

Due to those disadvantages, gas measurable RV-ADC in voltage domain is not matched with resistivity change measurable system in wide scale. On the other hand, measurement time of RP-FDC determines resolution of measurable value. Output change of sensor is not changed in a moment by gas concentration change under purpose of gas concentration measurement. As we see, there will be no big effect, despite of long sampling time due to slow change. Therefore, one of the advantages of RP-FDC-measurement time and resolution relationship has big advantage under purpose of gas concentration measurement.

1.4 Proposed system and target specification

In the case of [13], [14] thesis, control logic applied switched capacitor is used for frequency change adjustment based on resistivity size. Resolution can be adjusted through adjustment method of cycle scale in accordance with resistivity change section. Measurement time is fixed as bit of FDC is fixed. In other words, bit resolution of FDC is fixed as if bit resolution compatibility due to fixed counting time of FDC.

This thesis suggests time scale method on frequency counting adjustment of FDC counter. In the case of using Time scale, resolution can be adjusted in accordance with measurement purpose through measurement time adjustment of resistivity value.

Detailed target specification is shown below. Portable equipment alkaline battery is 2200mAH in the case of size between AA. Other parts of portable equipment such as MCU, display, speaker-driving power are mostly consumed. Below 0.5mW is designed including Oscillator and digital block. Measurement scales of 10K~50M ohm are set up to apply to most common gas sensor. Measurement time is set up to approximately 100ms as there is no need to measure tiny change of gas. Measurement resolution is set up to 12bit considering scale factor change and oscillator jitter. Refer to below table for Target performance.

Parameter	This work
Technology	0.18μm
Chip Area	0.5mm^2
Method	RP-FDC
Supply voltage	1V
Power Consumption	0.5mW
Measurement range	10K ~ 50M ohm
Measurement time	100ms below (typical)
Resolution	0.01ppm

Table 3: Target performance of proposed Resistance-to-Digital Converter

1.5 Oscillator

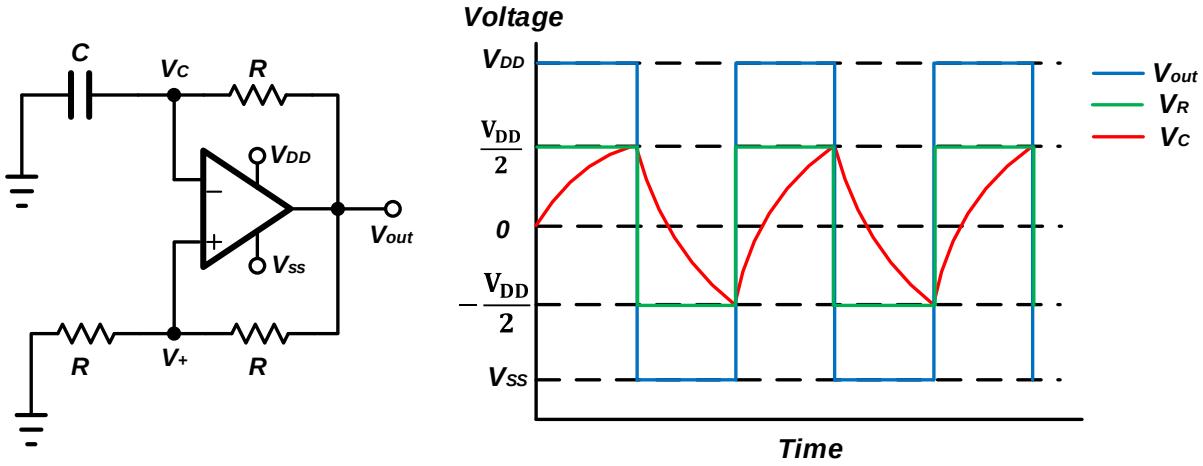

Figure 5: Basic Relaxation oscillator circuit

Relaxation oscillator: this oscillator makes unsquared wave such as square wave, a saw tooth wave, a chopping wave. An energy storage device such as capacitor or inductance and nonlinear switching device such as Schmitt Trigger compose feedback loop. Switching device makes signal through periodical repeat of storage device saved energy charge and discharge. Unsquared wave of relaxation oscillator is written with digital circuit clock.

1.5.1 Relaxation oscillator operation

In the case of identical value of Threshold voltage of OP AMP- V_+ to R, below is determined due to voltage distribution.

$$V_+ = \frac{V_{out}}{2} \tag{3}$$

Capacitor chargeable voltage can be found through a differential equation between chargeable voltage and current.

$$\frac{V_{out}-V_C}{R} = C\frac{dV_C}{dt} \tag{4}$$

Side arrangement of V_C looks like as below;

$$\frac{dV_C}{dt} + \frac{V_C}{RC} = \frac{V_{out}}{RC} \tag{5}$$

In the case of end of V_C charge and optional constant of A, the formula would be $\frac{dV_C}{dt} = 0$

$$\frac{A}{RC} = \frac{V_{out}}{RC} \tag{6}$$

Therefore $A = V_{out}$ is obtained. $V_C(K \cdot t) = V_{out}$, (in the time of V_C charge end as K is big enough during K·t time). If initial status is V_{out}= 0. The formula would be

$$\frac{dV_C}{dt} + \frac{V_C}{RC} = 0 \tag{7}$$

Variable isolation method is applied and $\frac{V_C}{RC}$ is moved to the right side and is rewritten as below;

$$dV_C = -\frac{V_C}{RC}dt \tag{8}$$

Both sides are divided in V_C and integral calculus is taken.

$$\int \frac{1}{V_C}dV_C = -\int \frac{1}{RC}dt \tag{9}$$

$$\ln V_C = -\frac{1}{RC}t + c \tag{10}$$

$$V_C = e^{-\frac{1}{RC}t+c} \tag{11}$$

Constant related parts are arranged as below;

$$V_C = C \cdot e^{-\frac{1}{RC}t} \tag{12}$$

Two types of value are written as below;

$$V_C(t) = V_{out} + C \cdot e^{-\frac{1}{RC}t} \tag{13}$$

Initial time of t=0 is equal to $V_C(0)$ =0 and V_{DD} is V_{DD}

$$0 = V_{DD} + C \tag{14}$$

Therefore, it is $C = -V_{DD}$. The formula is shown as below;

$$V_C(t) = V_{out} - V_{DD} \cdot e^{-\frac{1}{RC}t} \tag{15}$$

1.5.2 Oscillator frequency

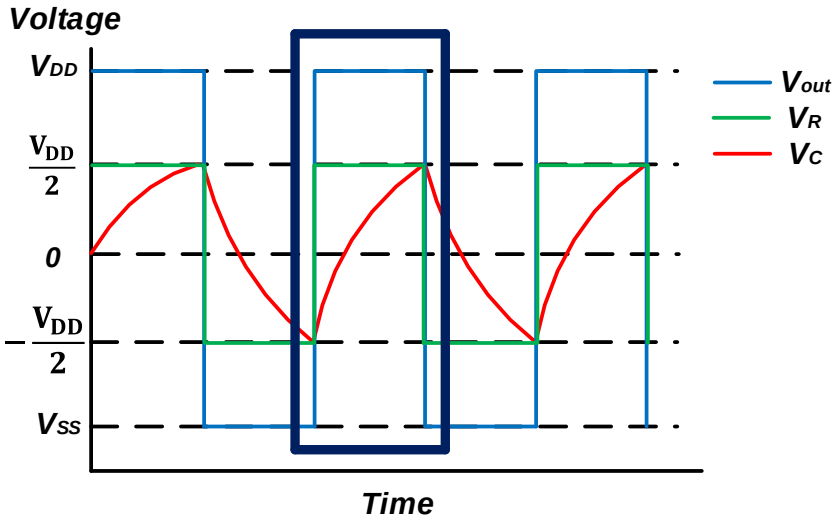

Figure 6: The signal during charge and discharge cycle

Assumption: Relaxation oscillator is ideal and threshold voltage is $\frac{V_{DD}}{2}$ and V_{SS} is $-V_{DD}$. Charge and discharge cycle is identical as T/2. Capacitor voltage repeats charge and discharge in $\frac{V_{DD}}{2}$.

Below formula can be modified in accordance with situation focusing on a box.

$$V_C(t) = V_{out} + \mathrm{B} \cdot e^{-\frac{1}{RC}t} \tag{16}$$

Charge starting initial, $V_{out} = V_{DD}$, t=0, $V_C = -\frac{V_{DD}}{2}$. Therefore

$$-\frac{V_{DD}}{2} = V_{DD} + \mathrm{B} \tag{17}$$

With $\mathrm{B} = -\frac{3V_{DD}}{2}$. If it is rewritten;

$$V_C(t) = V_{DD} - \frac{3V_{DD}}{2} \cdot e^{-\frac{1}{RC}t} \tag{18}$$

V_C is as below after half time pass of one cycle in charge cycle and the formula would be

$$\frac{V_{DD}}{2} = V_{DD} - \frac{3V_{DD}}{2} \cdot e^{-\frac{1}{RC}\cdot\frac{T}{2}} \tag{19}$$

Arranged formula would be

$$\frac{1}{3} = e^{-\frac{1}{RC}\cdot\frac{T}{2}} \tag{20}$$

The formula arranged to T would be

$$\ln\frac{1}{3} = -\frac{1}{RC}\frac{T}{2} \quad , \ \frac{\mathrm{T}}{2} = \mathrm{RC}\ln 3 \tag{21}$$

Therefore, the cycle would be $2\mathrm{RC}\ln 3$ and frequency would be $\frac{1}{2\mathrm{RC}\ln 3}$.

The cycle of ideal relaxation oscillator is determined by resistivity and capacitor. Convert resistivity change to frequency change using relaxation oscillator, which signal cycle is changed based on resistivity change for resistive gas sensor resistivity value measurement and frequency digitalization through FDC method is applied to RP-FDC is reasonable choice.

2. Background Information: Frequency Stability

This section explains the relationship between time domain and frequency domain in frequency stability aspect for noise interpretation. Frequency instability cannot be avoided in real oscillator and causes different result other than ideal frequency. Circuit design direction is known through interpretation about frequency instability. Finally, output noise effect can be predicted.

2.1 Time domain Basic definitions

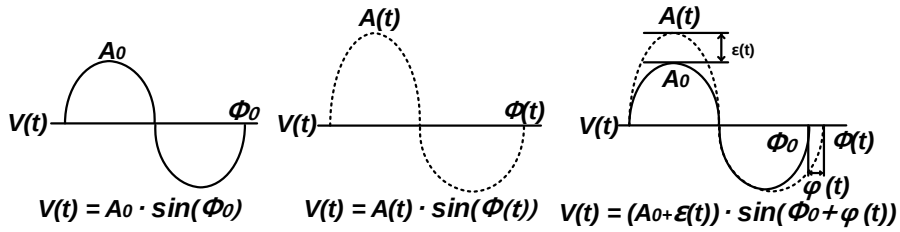

Figure 7: Ideal signal and noise signal

The practical periodic voltage signal (instantaneous voltage signal) can be written as:

$$\mathrm{V(t)} = \mathrm{A(t)} \cdot \sin\big(\Phi(t)\big) \tag{22}$$

$\mathrm{A(t)}$ is the instantaneous voltage amplitude and $\Phi(t)$ is the instantaneous phase. The amplitude voltage amplitude can be written as:

$$\mathrm{A(t)} = A_0 + \varepsilon(t) \tag{23}$$

A_0 is the ideal voltage amplitude and $\varepsilon(t)$ is the instantaneous voltage about A_0. The voltage fluctuation doesn't affect oscillator's phase in principle. The instantaneous phase can be written as:

$$\Phi(t) = \omega_0 t + \varphi(t) \tag{24}$$

ω_0 is the ideal angular frequency and it is a constant time derivative value of phase. $\varphi(t)$ is the random instantaneous phase fluctuation about the ideal phase $\omega_0 t$.

The instantaneous angular frequency is given by the time deviation of the instantaneous phase.

$$\omega(t) = \frac{d\Phi(\mathrm{t})}{dt} = \omega_0 + \frac{d\varphi(t)}{dt} = \omega_0 + \Delta\omega(t) \tag{25}$$

Angular frequency is equal to the change in the instantaneous phase over time. In other words, the amount of instantaneous phase changes is the integral of angular frequency. The instantaneous phase can be defined as ideal constant phase and random instantaneous angular frequency fluctuations. The instantaneous phase fluctuations over time is equal to the random instantaneous angular frequency fluctuations.

$$\frac{d\varphi(t)}{dt} = \Delta\omega(t) \tag{26}$$

The instantaneous fractional frequency fluctuation is defined as the ratio between ideal angular frequency ω_0 and instantaneous phase fluctuations over time $\frac{d\varphi(t)}{dt}$.

$$y(t) = \frac{\left(\frac{d\varphi(t)}{dt}\right)}{\omega_0} = \frac{\Delta\omega(t)}{\omega_0} = \frac{\Delta f(t)}{f_0} \tag{27}$$

Comparison about stability is possible even though frequency is different as the value is the proportion of error about normalcy. The random instantaneous phase-time fluctuation is related to phase instability, defined in terms of the instantaneous phase deviation $\varphi(t)$, can be expressed in units of time [15]:

$$x(t) = \frac{\varphi(t)}{\omega_0} \tag{28}$$

In other words, it is time error between affected time by ideal time cycle and noise. Fractional frequency fluctuation $y(t)$ of normalized frequency deviation can be written as below through (27), (28) formula.

$$y(t) = \frac{dx(t)}{dt} \tag{29}$$

2.2 Frequency domain Basic definitions

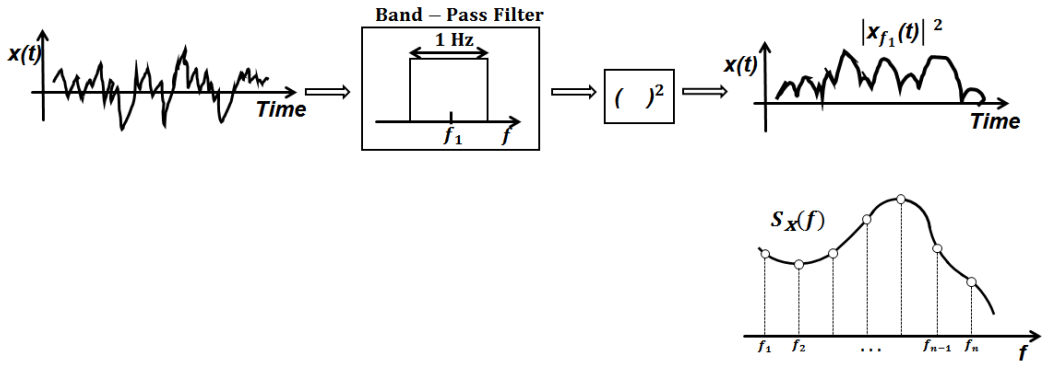

Figure 8: Noise signal to noise spectrum conversion

The power spectral density (PSD) is written for deciding frequency stability in frequency domain. PSD indicates power of every frequency signal. In other word, PSD-$S_x(f)$ of $x(t)$ signal is an average power, which is forwarded by $x(t)$ from bandwidth nearby frequency f. Noise signal- $x(t)$ is applied to band-pass filter, which have central frequency-f_1 and 1Hz bandwidth in Figure 8 and $S_x(f_1)$ filter output is obtained by square and average. The identical process is repeated for band-pass filter, which have different frequency as central frequency from f_2 to f_n and consequently $S_x(f)$ is obtained for all frequency [16].

Angular frequency fluctuation PSD $S_{\Delta\omega}(f)$, frequency fluctuation PSD $S_{\Delta f}(f)$, fractional frequency fluctuation PSD $S_y(f)$, phase fluctuation PSD $S_\varphi(f)$, and phase-time fluctuation PSD $S_x(f)$ are used for a frequency stability definition. In 2.1 section-defined, the relationship of time domain signal is seen in a frequency domain as below;

In (25), the relationship between the instantaneous phase fluctuation $\varphi(\mathrm{t})$ and the instantaneous angular frequency fluctuation $\Delta\omega(\mathrm{t})$ is expressed as PSD:

$$S_\varphi(f) = \frac{S_{\Delta\omega}(f)}{\omega^2} \tag{30}$$

In (27), the relationship between the fractional frequency fluctuation $\mathrm{y(t)}$ and the angular frequency fluctuation $\Delta\omega(\mathrm{t})$ is expressed as PSD:

$$S_y(f) = \frac{S_{\Delta\omega}(f)}{{\omega_0}^2} = \frac{S_{\Delta f}(f)}{{f_0}^2} \tag{31}$$

By using (30), (31), the fractional frequency fluctuation PSD can be expressed as:

$$S_y(f) = \frac{f^2}{{f_0}^2} S_\varphi(f) \tag{32}$$

Below picture specifies the relationship between time domain and frequency domain;

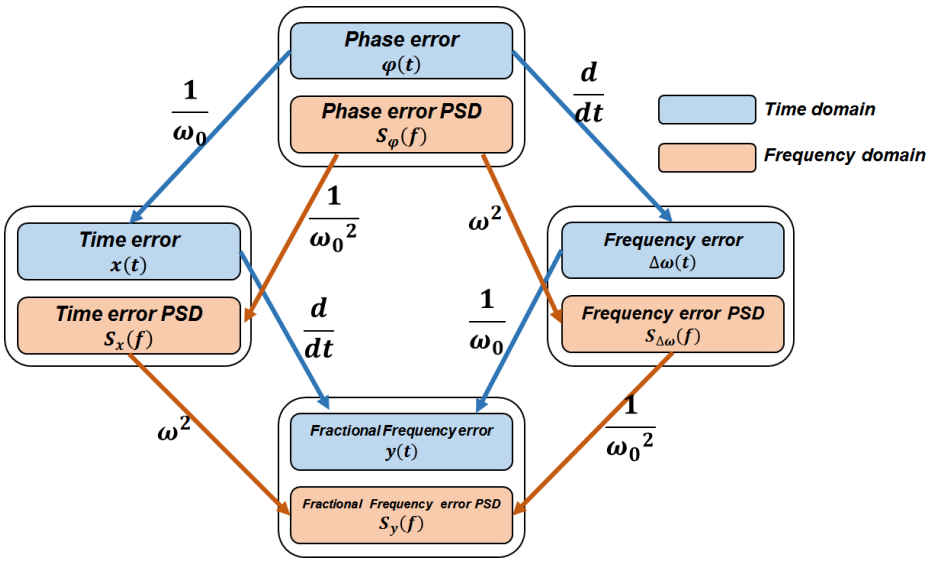

Figure 9: Relationship between Time domain and Frequency domain

2.3 Power-law noise models

The frequency and phase fluctuation can be modeled as power law curves. There is an advantage that practical results are matched in these models. This power-law model is expressed as the power spectral density of fractional frequency fluctuation $S_y(f)$ and instantaneous phase fluctuation $S_\varphi(f)$ [17] [18].

$$S_y(f) = \sum_{\alpha=-2}^{+2} h_\alpha \cdot f^\alpha \tag{33}$$

$S_y(f)$ can be indicated as below based on the relationship of (32).

$$S_\varphi(f) = \sum_{\alpha=-2}^{+2} {f_0}^2 \cdot h_\alpha \cdot f^{\alpha-2} \tag{34}$$

The number α is expressed as the slopes of each noise in log-log plot and describes the characteristic of noises. The constant h_α is the level of noises. There is a summary of the noise models in Table 4.

$S_y(f)$	α	Noise	$S_\varphi(f)$
$h_{-2} \cdot f^{-2}$	-2	Random walk frequency noise	${f_0}^2 \cdot h_{-2} \cdot f^{-4}$
$h_{-1} \cdot f^{-1}$	-1	Flicker frequency noise	${f_0}^2 \cdot h_{-1} \cdot f^{-3}$
h_0	0	White frequency noise	${f_0}^2 \cdot h_0 \cdot f^{-2}$
$h_1 \cdot f^1$	1	Flicker phase noise	${f_0}^2 \cdot h_1 \cdot f^{-1}$
$h_2 \cdot f^2$	2	White phase noise	${f_0}^2 \cdot h_2$

Table 4: Summary of noise models relationship

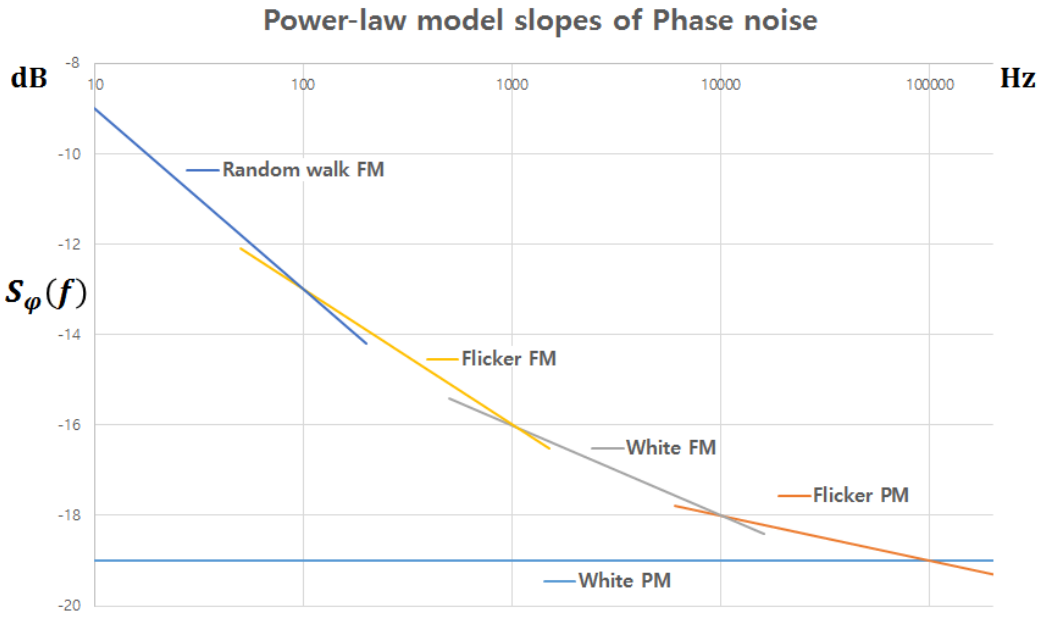

Figure 10: Power-law model slopes of phase noise

2.4 Wiener-Khinchine theorem

Below is the explanation of Wiener-Khinchine theorem, which helps to interpret random signal of time field in frequency field. In [19], the autocorrelation of a wide-sense-stationary random process by Fourier transformation is related to its power spectrum density. Above relationship can be indicated as below;

$$S_x(f) = \int_{-\infty}^{\infty} R_{xx}(\tau) e^{-j2\pi f t} d\tau \tag{35}$$

$R_{xx}(t)$ is the autocorrelation of wide-sense stationary random process $x(t)$.

2.5 Phase noise for designing oscillator

The signal of perfect cycle form is made in ideal oscillator. In other word, all zero-crossing occurs in integer ratio. However, it changes zero-crossing randomly by noise effect in real oscillator. Noise effect can be found in figure 7 of 2.1 section. In this case, phase noise $\varphi(t)$ is changed randomly based on time, in other word, waveform cycle is changed randomly by phase noise $\varphi(t)$. This phenomenon can be seen more intuitively in spectrum. In the case of $x(t) = A\cos[\omega_c t]$ signal, observation is possible in singular impulse form due to fixed cycle and in the case of $x(t) = A\cos[\omega_c t + \varphi(t)]$ signal, the cycle changes randomly and is indicated as out of ω_c. In a result, impulse is formed in broadened shape based on ω_c.

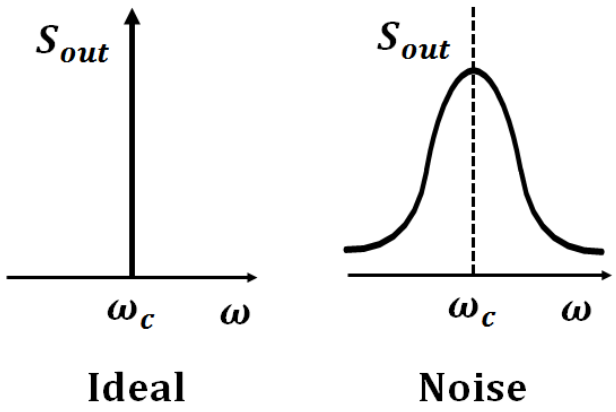

Figure 11: Ideal oscillator and noisy oscillator output spectrum

2.6 FOM (Figure of merit)

Figure-of-merit (FOM) is required for comparison between different oscillators such as operating power and operating frequency. FOM is the value, which considers trade-off among phase noise, frequency and power consumption and its definition shown below [20].

$$FOM = \frac{(Oscillation\ Frequency)^2}{Power\ Dissipation \times Phase\ noise \times (Offset\ Frequency)^2} \tag{36}$$

On the other hand, below formula is calculated in this thesis [21].

$$FOM = \left| L(\Delta f) + 20log\left(\frac{\Delta f}{f_0}\right) + 10\log\left(\frac{P_{diss}}{1mW}\right) \right| \tag{37}$$

$L(\Delta f)$, f_0, Δf, P_{diss} stands for phase noise in dBc/Hz, oscillation frequency, offset frequency, power consumption in mW.

$$FOM = \left| L(\Delta f) + 20log\left(\frac{\Delta f}{f_0}\right) + 10\log\left(\frac{P_{diss}}{1mW}\right) \right|$$

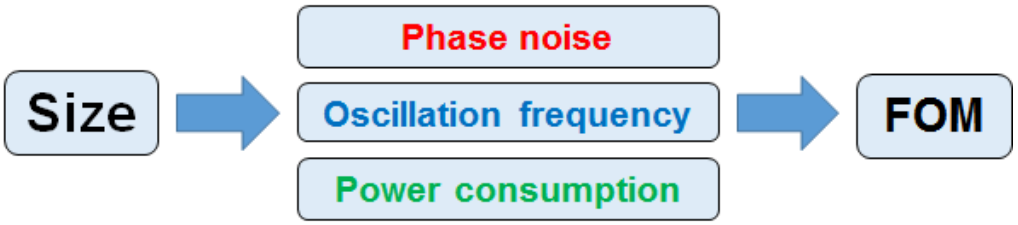

Figure 12: The relationship between size of inverter and FOM

To determine the size of inverter, the 3 factors, phase noise, oscillation frequency, and power consumption should be considered. That size separately affects that factors. When the size is increased, phase noise is going better. However, oscillation frequency is decreased and power consumption is increased. These three factors are linked each other. In these reason, FOM is meaningful factor to choose the inverter size.

3. Noise Analysis

Frequency stability of Oscillator in FDC included RP-FDC determines credibility of digital value. In addition, the frequency stability of oscillator can be predicted through noise interpretation of oscillator circuit. This section specifies about intuitive sense of layout direction through noise interpretation of oscillator.

3.1 Input referred noise of inverter

Determining part of the relaxation oscillator of this thesis is the inverter, which operates in the same way as a comparator. In the ideal case, V_{in} is bigger than $\frac{V_{DD}}{2}$, in the case of V_{in} is smaller than $\frac{V_{DD}}{2}$, V_{out} is printed out by V_{DD} or gnd. we are now going to look into how the inside noise ingredient of inverter can affect V_{in} input signal and finally, how it can affect stability of oscillator output.

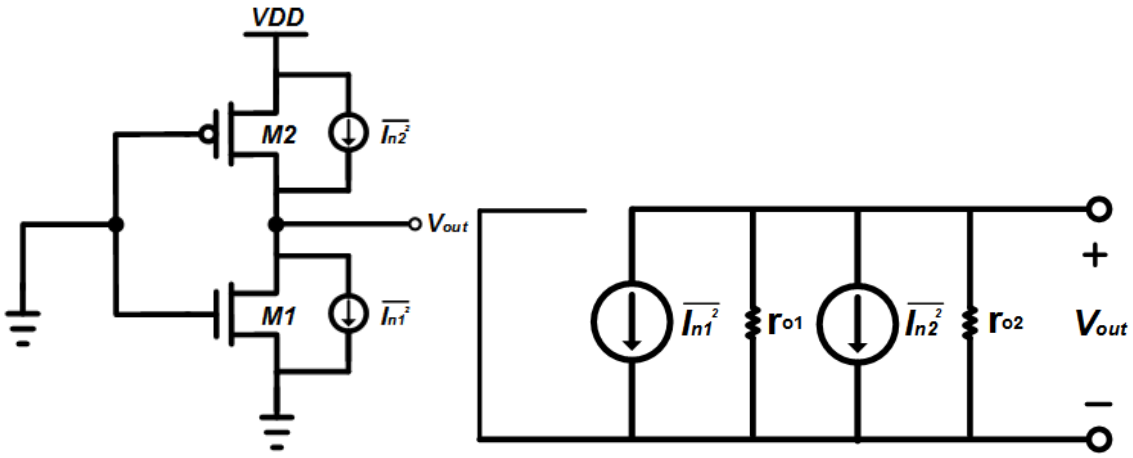

Figure 13: Small-signal model for input referred noise interpretation of the inverter.

Output noise voltage-$\overline{V_{n.out}^2}$ due to noise current shall be found for Input referred noise inducement by small-signal model.

$$\overline{V_{n.out}^2} = (\overline{I_{n1}^2} + \overline{I_{n2}^2})(r_{o1}//r_{o2})^2 \quad (38)$$

In this case, output resistivity is in parallel connection of r_{o1} and r_{o2}.

$$r_{out} = (r_{o1} \,//\, r_{o2}) \tag{39}$$

Therefore, the formula can be rewritten as below;

$$\overline{V_{n.out}}^2 = (\overline{I_{n1}}^2 + \overline{I_{n2}}^2) {r_{out}}^2 \tag{40}$$

Besides, it divides to a system gain based on Input referred noise definition. The profit is shown below;

$${A_V}^2 = (g_{m1} + g_{m2})^2 \cdot {r_{out}}^2 \tag{44}$$

$$\overline{V_{n,in}}^2 = (\overline{I_{n1}}^2 + \overline{I_{n2}}^2)\left(\frac{1}{g_{m1}+g_{m2}}\right)^2 \tag{45}$$

g_{m1} and g_{m2} are identical in the case of identical size of M1 and M2. And the input referred noise can be written as below;

$$\overline{V_{n,in}}^2 = \frac{1}{4}\overline{I_{n1}}^2 + \frac{1}{4}\overline{I_{n1}}^2 \tag{46}$$

As a result, the input referred noise of inverter on flicker noise and thermal noise, which occur in transistor, are shown as below table. The size of M1 and M2 are deemed as similar. ($W_1 = W_2,\ L_1 = L_2$)

	Flicker noise	**Thermal noise**
Voltage spectral density	$\frac{K}{C_{ox}fWL}$	$\frac{4kT\gamma}{g_m}$
Current spectral density	$\frac{K}{C_{ox}fWL}{g_m}^2$	$4kT\gamma g_m$
Input referred noise (voltage)	$\frac{1}{2}\frac{K}{C_{ox}fWL}$	$\frac{2kT\gamma}{g_m}$
Input referred noise (current)	$\frac{1}{2}\frac{K}{C_{ox}fWL}{g_m}^2$	$2kT\gamma g_m$

Table 5: Flicker noise and thermal noise of transistor, input referred noise of inverter

3.2 Noise contribution to Phase noise

In section 3.1, we looked into how the inverter affects with input voltage noise. In this section, we are going to look into how input voltage noise consequently affects with oscillator phase noise. Overall inducement process shows below;

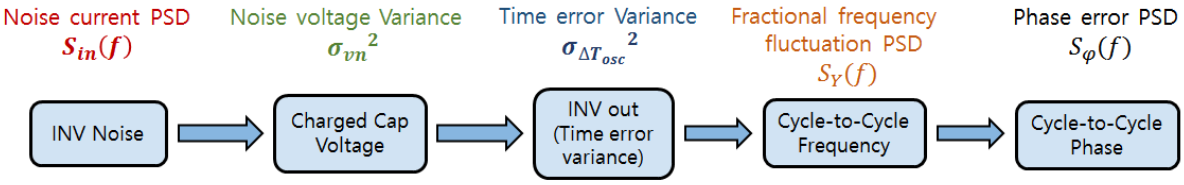

Figure 14: Flow chart of overall noise interpretation.

3.2.1 Noise current fed to a capacitor

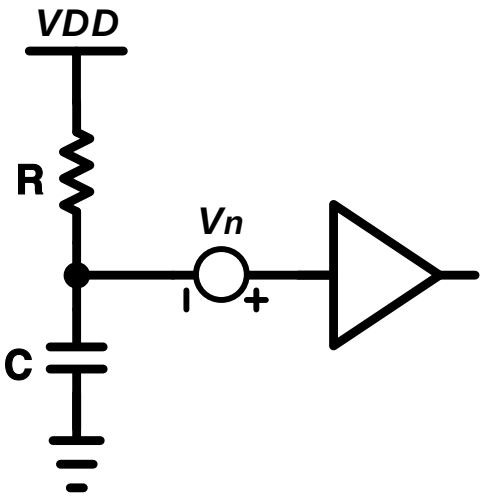

Figure 15: Simplified RC oscillator

In section 3.1, we looked into input referred form indication of the inside noise of the inverter. In consideration of current source form, we got to know about noise current source charge to capacitor in the charge cycle of relaxation oscillator.

Charging voltage during T_{charge} charge cycle to capacitor by i_n voltage can be written as below.

$$v(t) = \frac{1}{C_L}\int_{t-T_{charge}}^{t} i_n(t)dt \tag{47}$$

In addition, above formula can be modified in convolution form using a system function.

$$v(t) = \frac{1}{C_L}\int_{-\infty}^{\infty} i_n(p) \cdot h_I(t-p)dp \tag{48}$$

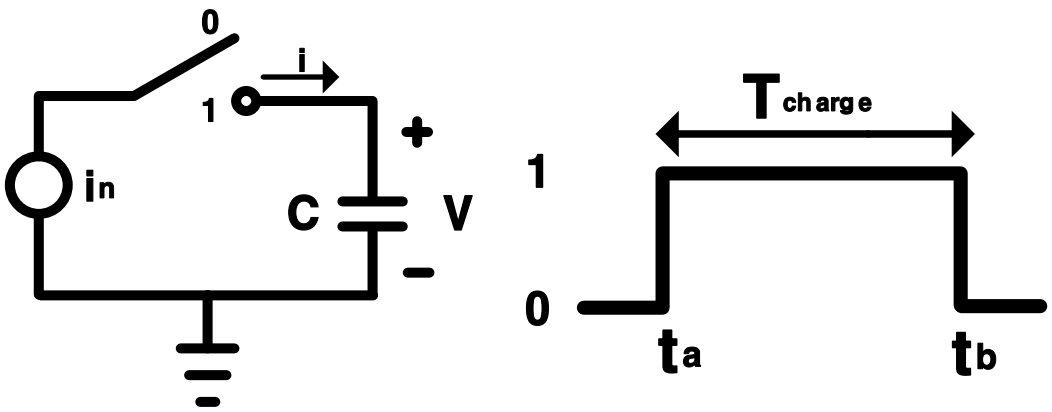

Figure 16: Voltage charging process of capacitor

In this case, voltage can flow after switch is ON of t_a time of below shown picture and voltage flow is stopped once switch is OFF of t_b time. A system function applied formula shown below;

$$h_I(t) = 1 \ (0 \le t \le T_{charge}) \tag{49}$$

$$= 0 \text{ (else)}$$

In the case of moving $h_I(t)$ system function to a frequency field through Fourier transform, below formula can be indicated.

$$|H_I(f)|^2 = \left[T_{charge} \cdot \frac{\sin(\pi f T_{charge})}{\pi f T_{charge}}\right]^2 \tag{50}$$

In the case of indicating $v(t)$ charging voltage of capacitor in power spectral density, below formula can be indicated.

$$S_{vn}(f) = \frac{1}{{C_L}^2} \cdot S_{in}(\mathrm{f}) \cdot |H_I(f)|^2 \tag{51}$$

In frequency domain, the voltage noise variance can be achieved by integration over all frequencies of the output voltage power spectral density.

$$\sigma_{vn}{}^2 = \int_0^\infty S_{vn}(f)df \tag{52}$$

$$\sigma_{vn}{}^2 = \frac{S_{in}(\mathrm{f})}{C_L{}^2}\int_0^\infty \left[T_{charge}\cdot\frac{\sin(\pi f T_{charge})}{\pi f T_{charge}}\right]^2 df \tag{53}$$

Below simple formula can be written in the case of solving the formula.

$$\sigma_{vn}{}^2 = \frac{1}{C_L{}^2}\frac{S_{in}}{2}T_{charge} \tag{54}$$

3.2.2 Voltage noise to Time error variance

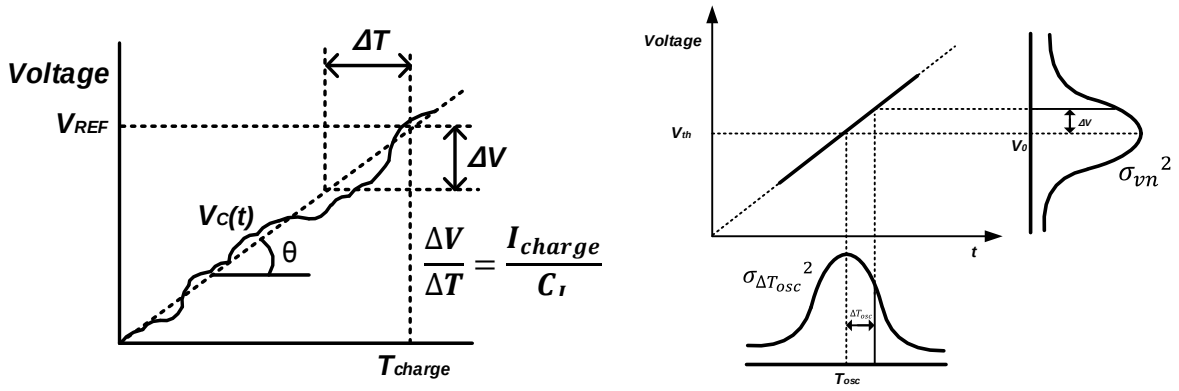

Figure 17: Capacitor voltage in charging period, Relationship between voltage variance and time error variance

We have already found the input referred noise of the inverter. Inside inverter is expressed as noiseless circuit while finding the input referred noise. Also, comparator-operating inverter has intrinsic threshold voltage. In the case of expressing intrinsic threshold voltage as V_{REF} in noiseless circuit, V_{REF} can be seen as fixed value, which is not affected by noise. In other word, the result of frequency stability through inverter can be affected by only input voltage variance.

In other word, the ratio of input voltage deviation and time deviation is identical with charging voltage grade of capacitor.

$$\frac{dV_C}{dt} = \frac{\Delta V_C}{\Delta T} = \frac{\sigma_{V_n}}{\sigma_{\Delta T}} = \frac{I_{charge}}{C} \tag{55}$$

The relationship between input voltage deviation and time deviation can written as below;

$$\left(\frac{dV_C}{dt}\right)^2 = \frac{{\sigma_{V_n}}^2}{{\sigma_{\Delta T}}^2} \tag{56}$$

Below formula can be rewritten for time error variance consideration by input voltage variance.

$${\sigma_{\Delta T}}^2 = \frac{{\sigma_{V_n}}^2}{\left(\frac{dV_C}{dt}\right)^2} = {\sigma_{V_n}}^2 \left(\frac{dt}{dV_C}\right)^2 \tag{57}$$

Time error variance can be found by applying input voltage variance and relationship between input voltage deviation and time deviation.

$${\sigma_{\Delta T}}^2 = \frac{1}{{C_L}^2}\frac{S_{in}}{2}T_{charge} \cdot \left(\frac{C_L}{I_{charge}}\right)^2 = \frac{S_{in}}{2}\frac{T_{charge}}{{I_{charge}}^2} \tag{58}$$

In the case of writing ΔT, which stands for charging cycle time error as ΔT_{osc}, which stands for single cycle error, and modifying T_{charge} as T_{osc}, the result looks like as below;

$${\sigma_{\Delta T_{osc}}}^2 = \frac{S_{in}}{2}\frac{T_{osc}}{{I_{charge}}^2} \qquad (T_{charge} = 0.5T_{osc},\ {\sigma_{\Delta T_{osc}}}^2 = 2{\sigma_{\Delta T}}^2) \tag{59}$$

As a result, time error variance about input referred noise of inverter can be arranged as below table;

	Flicker noise	**Thermal noise**
Input referred noise (current)	$\frac{1}{2}\frac{K}{C_{ox}fWL}{g_m}^2$	$2kT\gamma g_m$
Time error variance	$\frac{1}{4}\frac{K \cdot {g_m}^2}{C_{ox}fWL}\frac{T_{osc}}{{I_{charge}}^2}$	$kT\gamma g_m \cdot \frac{T_{osc}}{{I_{charge}}^2}$

Table 6: Relationship between input referred noise of inverter and time error variance

3.2.3 Time error variance to fractional frequency fluctuation

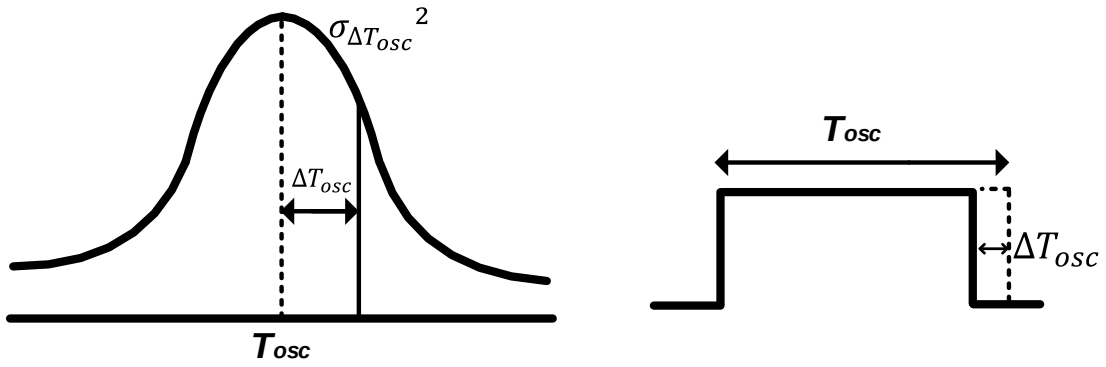

Figure 18: Time error variance and deviation

In prior to explain the relationship between time error variance and fractional frequency fluctuation, we shall look into the relationship between time error deviation $\frac{\sigma_{\Delta T_{osc}}}{T_{osc}}$ of single cycle and frequency error deviation.

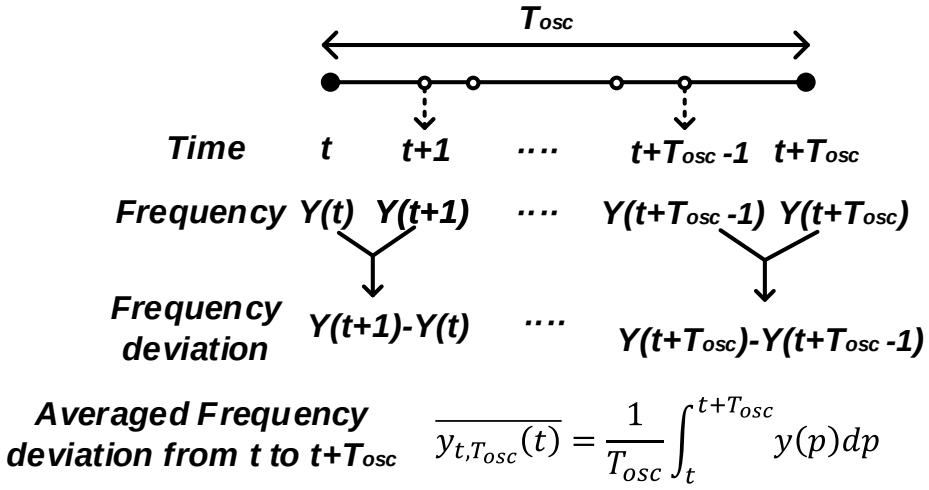

Figure 19: Averaged frequency deviation within time interval

Our purpose is to measure frequency stability in time domain. The frequency stability is measured through frequency deviation average, which has been changed during T_{osc} time interval. Averaged frequency deviation can be written as below by the relationship between random phase-time fluctuation x(t) and random fractional frequency fluctuation y(t) in time domain.

$$\overline{y_{t,T_{osc}}(t)} = \frac{\varphi(t+T_{osc})-\varphi(t)}{2\pi f_0 T_{osc}} = \frac{1}{T_{osc}}[x(t+T_{osc}) - x(t)] \quad (60)$$

Below relationship is established as averaged frequency deviation $\overline{y_{t,T_{osc}}(t)}$ is the random variation.

$$\sigma\left[\overline{y_{t,T_{osc}}(t)}\right]^2 = \overline{y_{t,T_{osc}}(t)^2} \quad (61)$$

Therefore, $\overline{y_{t,T_{osc}}(t)}$ can be arranged as below;

$$\sigma\left[\overline{y_{t,T_{osc}}(t)}\right] = \frac{1}{T_{osc}}[x(t+T_{osc}) - x(t)] = \frac{1}{T_{osc}}[\Delta T_{osc}] = \frac{\sigma_{\Delta T_{osc}}}{T_{osc}} \quad (62)$$

Above-mentioned averaged frequency deviation can be modified in system function applied convolution form.

$$\sigma\left[\bar{y}_{t,T_{osc}}\right] = \frac{1}{T_{osc}}\int_t^{t+T_{osc}} y(p)dp = \int_{-\infty}^{\infty} y(p)\cdot h_i(t-p)dp \quad (63)$$

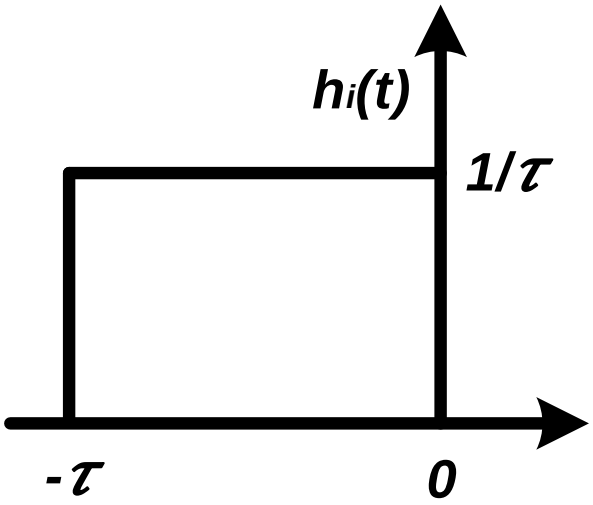

Figure 20: System transfer function

In this case, a single cycle average system forwarding $h_i(t)$ function can be indicated as below;

$$h_i(t) = \frac{1}{\tau} \ (-\tau \le t \le 0) \quad (64)$$

$$= 0 \ (else)$$

$h_i(t)$ system forwarding function is converted to frequency field in time field for calculation of convolution in frequency field.

$$|H_I(f)|^2 = \left[\frac{\sin(\pi f T_{osc})}{\pi f T_{osc}}\right]^2 \quad (65)$$

The convolution calculation in frequency field shown below;

$$\sigma\left[\bar{y}_{t,T_{osc}}\right]^2 = \int_0^\infty S_y(f) \cdot |H_I(f)|^2 df = \int_0^\infty S_y(f) \cdot \left|\frac{\sin(\pi f T_{osc})}{\pi f T_{osc}}\right|^2 df = S_y(f) \cdot \frac{1}{2T_{osc}} \quad (66)$$

Below formula is about fractional frequency fluctuation PSD $S_y(f)$ as knowing frequency stability is the purpose.

$$S_y(f) = 2T_{osc} \cdot \sigma\left[\bar{y}_{t,T_{osc}}\right]^2 \quad (67)$$

Below formula is indicated by applying relationship between averaged frequency deviation and normalized time error deviation.

$$S_y(f) = 2T_{osc} \cdot \left(\frac{\sigma_{\Delta T_{osc}}}{T_{osc}}\right)^2 \quad (68)$$

As a result, fractional frequency fluctuation PSD $S_y(f)$ about time error variance of inverter output is arranged as below table;

	Flicker noise	**Thermal noise**
Time error variance	$\frac{1}{4}\frac{K \cdot {g_m}^2}{C_{ox} f W L}\frac{T_{osc}}{{I_{charge}}^2}$	$kT\gamma g_m \cdot \frac{T_{osc}}{{I_{charge}}^2}$
Fractional frequency fluctuation PSD	$\frac{1}{2}\frac{K \cdot {g_m}^2}{C_{ox} f W L}\frac{1}{{I_{charge}}^2}$	$2kT\gamma g_m \frac{g_m}{{I_{charge}}^2}$

Table 7: Relationship between time error variance and fractional frequency fluctuation PSD

3.2.4 Fractional frequency fluctuations to Phase error

Domain relationship in previous section is applied for converting Fractional frequency fluctuation PSD $S_y(f)$ to Phase error PSD $S_\varphi(f)$. Firstly, fractional frequency fluctuation PSD $S_y(f)$ is converted to frequency error PSD $S_{\Delta\omega}(f)$ and conversion is processed by applying frequency error PSD $S_{\Delta\omega}(f)$ and Phase error PSD $S_\varphi(f)$

relationship.

Firstly, the frequency error ratio of all frequencies can be indicated as below;

$$y(\mathrm{t}) = \frac{\Delta f(t)}{f_0} = \frac{\Delta\omega(t)}{\omega_0} \tag{69}$$

Therefore, above formula can be written as below, in the case of modifying the formula through Fourier transform.

$$S_y(f) = \frac{S_{\Delta\omega}(f)}{{\omega_0}^2} \tag{70}$$

We are now going to look into the relationship between frequency error and phase error. The instantaneous angular frequency is expressed as the sum of ideal constant angular frequency and the random instantaneous angular frequency fluctuation.

$$\omega(\mathrm{t}) = \omega_0 + \Delta\omega(t) = \omega_0 + \frac{d\varphi(t)}{dt} \tag{71}$$

$\Delta\omega$, which stands for very time random change of angular frequency, is identical as phase deviation of momentary time. In other words, the relationship between two can be modified as below;

$$\Delta\omega(t) = \frac{d\varphi(t)}{dt} \tag{72}$$

In Fourier transform, deviation is calculated as below;

$$F\left[\frac{df(t)}{dt}\right] = \int_{-\infty}^{\infty} \frac{df(t)}{dt} e^{-j\omega t} dt = -j\omega \int_{-\infty}^{\infty} f(t)\, e^{-j\omega t} dt \tag{73}$$

The relationship between two are converted in frequency field. Square is taken to both sides and Fourier transform is processed. The relationship between frequency error and phase error is induced in frequency field as below. Negative number is omitted as both sides are symmetric based on 0 frequency of frequency in power spectral density.

$$S_{\Delta\omega}(f) = \omega^2 S_{\varphi}(f) \tag{74}$$

Fractional frequency fluctuation PSD $S_y(f)$ is converted to Phase error PSD $S_{\varphi}(f)$ based on the formula shown above.

$$S_\varphi(f) = \frac{{\omega_0}^2}{\omega^2} S_y(f) \tag{75}$$

As a result, above-mentioned relationship is arranged as below and Phase error PSD $S_\varphi(f)$ of fractional frequency fluctuation PSD $S_y(f)$ is shown in below table;

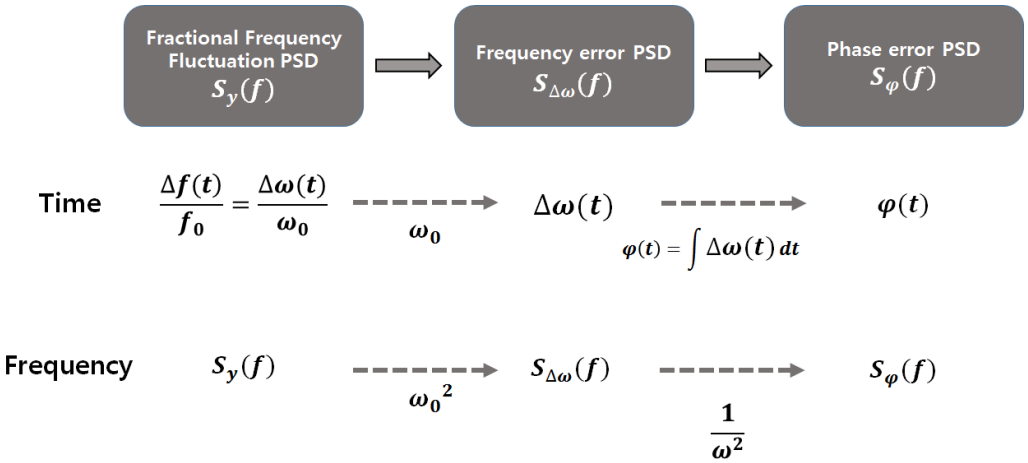

Figure 21: Fractional frequency fluctuations to phase error derivation

	Flicker noise	**Thermal noise**
Fractional frequency fluctuation PSD	$\frac{1}{2}\frac{K \cdot {g_m}^2}{C_{ox} f W L}\frac{1}{{I_{charge}}^2}$	$2kT\gamma g_m \frac{g_m}{{I_{charge}}^2}$
Phase error PSD	$\frac{1}{2}\frac{K \cdot {g_m}^2 \cdot {f_0}^2}{C_{ox} f^3 W L}\frac{1}{{I_{charge}}^2}$	$\frac{2kT\gamma \cdot {f_0}^2}{f^2}\frac{g_m}{{I_{charge}}^2}$

Table 8: Relationship between fractional frequency fluctuation PSD and phase error PSD

3.2.5 Phase error to Phase noise

Phase noise of old definition was the ratio of power density in one phase noise modulation sideband per 1Hz on total signal power [15].

$$L(f)_{total} = \frac{power\ density\ in\ one\ phase\ noise\ modulation\ sideband,per\ 1Hz}{Total\ signal\ power} = \frac{P_{sideband}(f_0+f,1Hz)}{P_{carrier}} \quad (76)$$

The power in above definition includes the effect by amplitude and phase fluctuation and this thesis considers only the effect of phase fluctuation. Therefore, the formula can be modified as below;

$$L(f) = \frac{P_{\varphi-sideband}(f_0+f,1Hz)}{P_{carrier}} \quad (77)$$

The $P_{\varphi-sideband}(f_0+f,1Hz)$ is the power per 1 Hertz bandwidth in one phase modulation sideband of the single sided spectrum of the oscillator signal, at a frequency offset f from the carrier frequency f_0 [22]. In [22], the new definition is proposed in terms of $S_\varphi(f)$.

$$L(f) = \frac{S_\varphi(f)}{2} \quad (78)$$

Phase noise $L(f)$ of Phase error PSD $S_\varphi(f)$ is proposed as below table;

	Flicker noise	**Thermal noise**
Phase error PSD	$\frac{1}{2}\frac{K\cdot {g_m}^2\cdot {f_0}^2}{C_{ox}f^3WL}\frac{1}{{I_{charge}}^2}$	$\frac{2kT\gamma\cdot {f_0}^2}{f^2}\frac{g_m}{{I_{charge}}^2}$
Phase noise	$\frac{1}{4}\frac{K\cdot {g_m}^2\cdot {f_0}^2}{C_{ox}f^3WL}\frac{1}{{I_{charge}}^2}$	$\frac{kT\gamma\cdot {f_0}^2}{f^2}\frac{g_m}{{I_{charge}}^2}$

Table 9: Relationship between Phase error PSD and Phase noise

4. System Structure & Operation principle

This section looks into operation principle and overall composition of system. Besides, this section also looks into feature per block and output change due to features.

4.1 Structure Block diagram

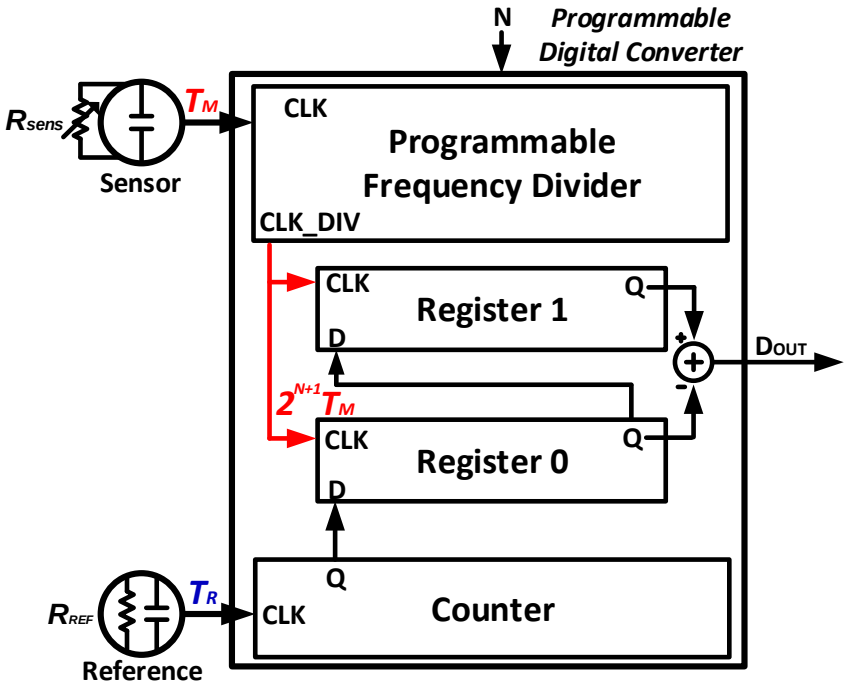

Figure 22: Block diagram of the proposed resistance-to-digital converter

Above is the thesis proposed resistance-to-digital converter diagram. The resistance-to-digital converter is consisted of two relaxation oscillator and Frequency-to-digital converter. Relaxation oscillator is consisted of measurement oscillator, which makes frequency through on-chip capacitor and gas sensor by external resistance role and reference oscillator, which forms fixed frequency through on-chip resistor and capacitor. Two on-chip capacitor C_M, C_R are the identical value. Therefore, the ratio of two T_M, T_R time cycle, which are made in oscillator, is determined as only resistivity ratio.

Frequency-to-Digital converter (FDC) is consisted of programmable Frequency divider, register, counter. Programmable frequency divider (PFD) takes care of dividing changeable measurement frequency in accordance with divider factor based on gas sensor. The free-running counter divides and inputs clock of reference oscillator

per stage of register. Register saves current cycle value and previous cycle value for baseline cancelation.

4.2 Details of each block

This section looks into every block, which contains all system. The section also looks into operation principle and purpose of every bock and it also looks into how those are connected and operated organically.

4.2.1 Relaxation oscillator

In this section, we are going to look into this thesis proposed structure but not relaxation oscillator of simple structure, which was explained in introduction.

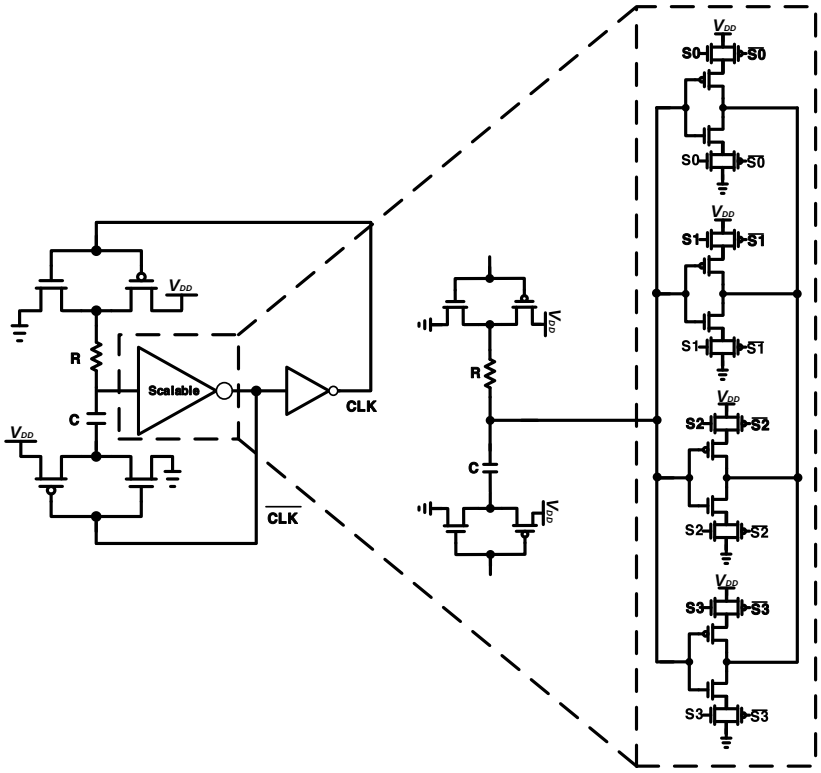

Figure 23: Schematic of the relaxation oscillator

The proposed relaxation oscillator is able to adjust the size of inverter through exterior enable signal. Refer to previous noise interpretation for the meaning of scalable method of inverter in relaxation oscillator. The inverter, which is located after RC in relaxation oscillator structure, is the part to determine oscillator cycle of inverter.

The scalable inverter is proposed for reducing the time error (jitter). Jitter is the corrupted time period by phase noise in time domain. In chapter 3, we already cover the relationship between circuit noises and time error. According to Table 6, Flicker noise, one of the noise source, contributes to time error and that is determined by the size of inverter. In this reason, the scalable inverter is able to adjust the jitter. For frequency-to-digital converter, frequency stability limits the resolution of digital value.

The resolution of digital block is determined by scale factor N (Equation 86). When measurement oscillation frequency is high, narrow measurement window makes the conversion time short. In this case, to increase the resolution of digital output value, people increases the scale factor N. Then, increased scale factor makes the resolution high and jitter limits the resolution. Because the minimum measureable period should be larger than time error (jitter).

The jitter in time domain is similar to the voltage noise in voltage domain. In voltage domain, the minimum achievable digital output should be larger than voltage noise. It is for avoiding the uncertain value that is randomly generated by voltage noise. In this reason, in time domain the minimum achievable digital output should be larger than jitter. Frequency-to-digital converter needs to reduce the jitter, when high resolution is wanted.

When measurement oscillator's oscillation frequency is high, large size of inverter is required for reducing the jitter. For low oscillation frequency, wide range of measurement period limits the increasing scale factor. Because at low frequency, measurement period is already wide. Additional increased scale factor can make the excessively extended measurement time. Therefore, at low frequency, jitter is less dominant than power consumption. As a result, scalable inverter can make the inverter size adjustable and it can optimize the digital converter performance depending on measurement frequency.

One more advantage, Swing-boosting effect can be obtained thanks to above structure. The location of series RC circuit V_{DD} and gnd are changed by turns during charge and discharge cycle as shown below. In this case, V_1, which is saved during charging cycle, is added to V_{DD}, which is saved during discharging cycle and discharge is started from $V_{DD} + V_1$. V_C voltage gets lower V_2 than V_{DD} after discharge is finished. The voltage of charge starting begins from $-V_2$, lower than 0V voltage in recharging cycle start process. Voltage become V_3, higher than 0V after charging is finished. In other word, periodic location shifts of V_{DD} and gnd helps obtaining Swing-boosting effect when the voltage width is bigger than power width in charge and discharge of capacitor process.

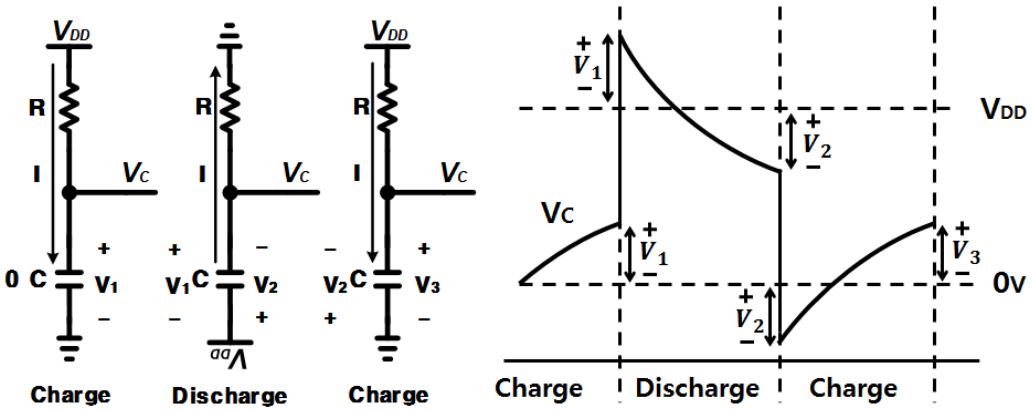

Figure 24: Charge-Discharge phase and Swing-Boosted effect

In the case of applying above-mentioned swing-boosting effect to inverter, which has relaxation oscillator voltage, charging and recharging capacitor can be indicated as below;

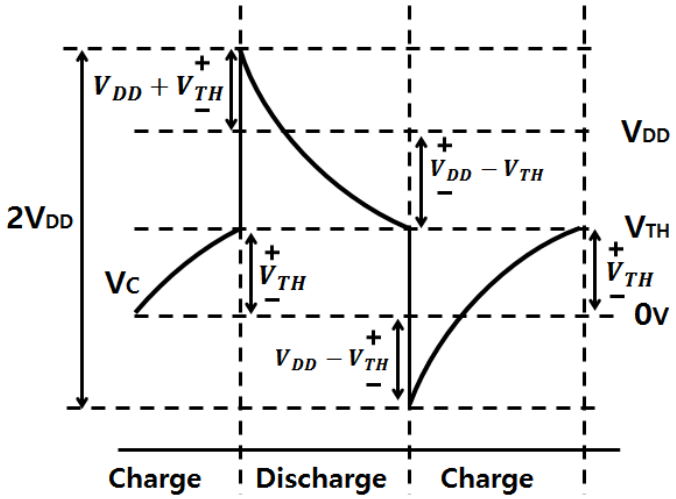

Figure 25: Swing-Boosted effect in relaxation oscillator

As a result, if ideal intrinsic threshold voltage is equal to $\frac{V_{DD}}{2}$, charging and discharging voltage scale of capacitor by swing-boosting effect would be equal to $2V_{DD}$. Now, let us look at the advantage of inverter input, which made frequency, by charging bigger voltage of capacitor than input voltage. Below is the situation, in which optional threshold exists and threshold voltage is changed randomly by noise.

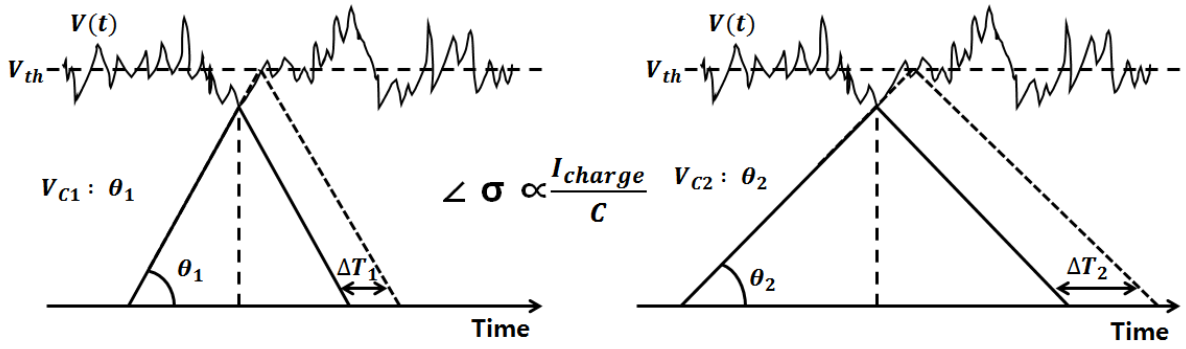

Figure 26: The relationship between current source and time error

Let us suppose that there are different voltages such as V_{C1}, V_{C2} of capacitor charging and discharging voltage. Input voltage of V_{C1} is bigger than V_{C2}. Let us compare the left side shown picture, in which reaching time to polluted V_{TH}- V(t) at noise while V_{C1} is charging and ideal time difference-ΔT_1 of V_{TH} reaching time than the right side time shown picture, in which time difference-ΔT_2 made by V_{C2}. In the case of high input voltage of inverter, time error by noise may decrease relatively. Therefore, in the case of increasing capacitor charging and discharging scale to $2V_{DD}$, time error size would decrease than V_{DD} original charging and discharging voltage scale, by applying swing-boosting technic.

4.2.2 Programmable frequency divider

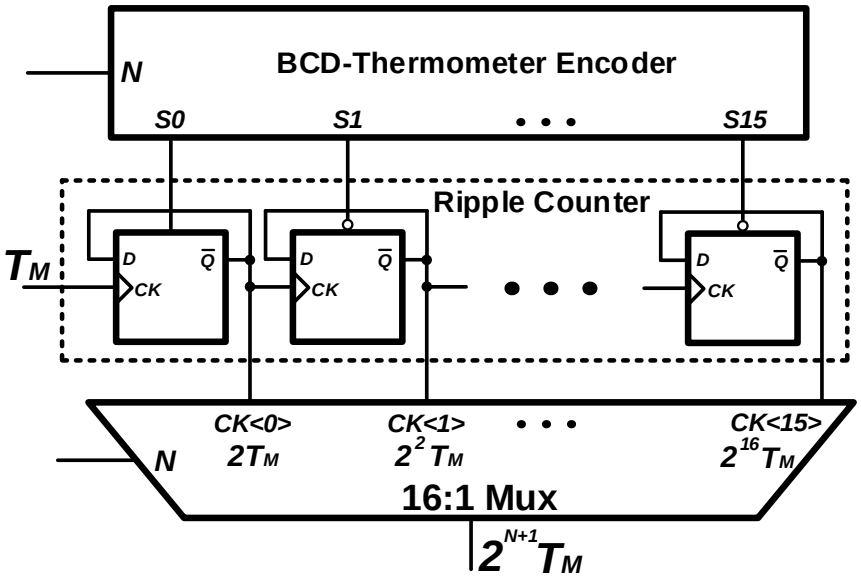

Figure 27: Programmable frequency divider

Programmable frequency divider is the block, which takes care of cycle T_M increase made from measurement oscillator in accordance with scalable factor. Programmable frequency divider is consisted of BCD-Thermometer Encoder and Ripple Counter, Mux. In the case of binary formed scalable factor input from outside, output is occurred by 4bit Binary related decimal location between D0~D15 binary-to-decimal converter of inside BCD-Thermometer Encoder. Thermometer, in accordance with block role, takes care of all output occurrence of below decimal size, which is input entered.

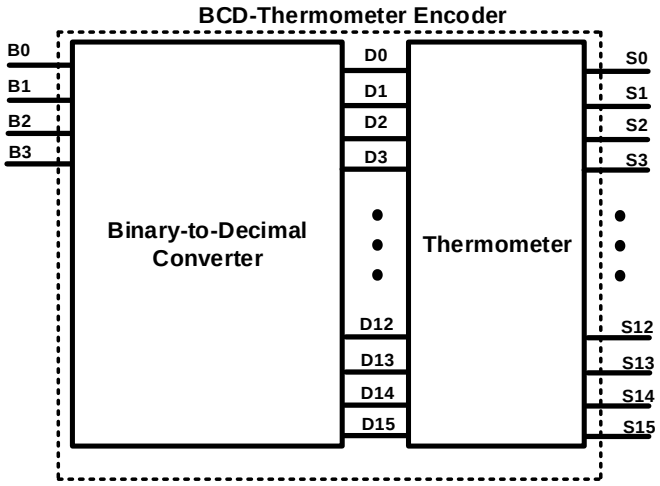

Figure 28: BCD-Thermometer Encoder

The output of thermometer operates with enable signal of ripple counter and causes the effect of period increase. Then, it outputs scale factor related point result in mux. As a result, output cycle can be rewritten as the relationship between scale factor and measurement period as below;

$$T_{PFD} = 2^{N+1} T_M \tag{79}$$

4.2.3 Free-running counter, registers, adder

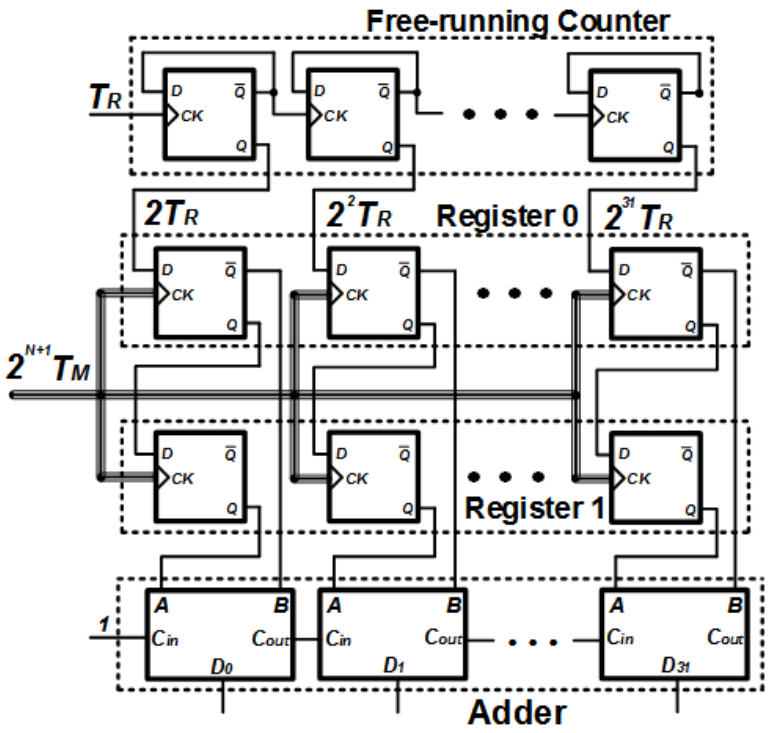

Figure 29: Free-running counter, registers, adder

Below are blocks, which counts cycle and saves value. The blocks are consisted of free-running counter, registers, and adder. Fixed cycle from Reference oscillator is input by Free-running counter. The cycle is lengthened two times per stage through flip-flop. Lengthened cycle is saved in register and is converted by being added as two's complement form in value and adder of next cycle. The specified process due to digital output will be explained in the next section.

4.3 Measurement operation and equations

In this section, we are going to look into how the operation of every block affects final output. Below shown picture explains the measurement of situation, in which measurement time is increased as $2^{N+1}T_M$ by scale factor of measurement period.

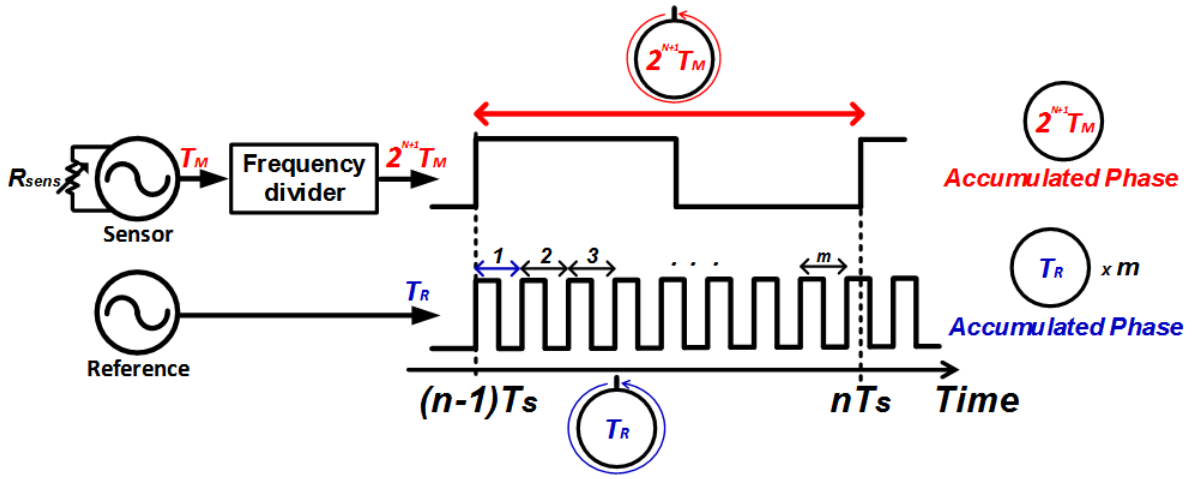

Figure 30: RCD timing diagram in time domain

It measures T_R repeat frequency during measurement time. Total added status by T_R during measurement time can be found as below;

$$\varphi_{sum}(T_s) = \int_{(n-1)T_s}^{nT_s} 2\pi \left(\frac{1}{T_R}\right) dt = \int_{(n-1)T_s}^{nT_s} 2\pi \left(\frac{1}{2R_R C_R}\right) dt \tag{80}$$

The total added status by $nT_S \sim (n-1)T_S$, T_R is identical with added status during $2^{N+1}T_M$ measurement time.

$$\varphi_{sum}(T_s) = \int_{(n-1)T_s}^{(n-1)T_s + 2^{N+1}T_M} 2\pi \left(\frac{1}{2R_R C_R}\right) dt = 2\pi \left(\frac{2^{N+1} 2R_M C_M}{2R_R C_R}\right) \tag{81}$$

In the case of identical fixed capacitor C_R and C_M inside current, the formula can be proposed as below;

$$\varphi_{sum}(T_s) = 2\pi \left(\frac{2^{N+1} R_M}{R_R}\right) \tag{82}$$

In other word, it is indicated as ratio between reference resistivity and measurement resistivity. Combined status is divided with 2π and is indicated as the section of cycle.

$$D_{OUT} = \frac{2^{N+1} R_M}{R_R} \tag{83}$$

PVT variation insensitive effect can be expected through below expressed digital output form. α_M, α_R temperature constant and β_M, β_R voltage constant and γ_M, γ_R process constant exist. Let us suppose effect by ΔT exterior temperature change, ΔV input voltage change and ΔP process variation effect.

$$D_{OUT(\Delta T, \Delta V, \Delta P)} = \frac{2^{N+1} R_M (1+\alpha_M \Delta T)(1+\beta_M \Delta V)(1+\gamma_M \Delta P)}{R_R (1+\alpha_R \Delta T)(1+\beta_R \Delta V)(1+\gamma_R \Delta P)} \approx \frac{2^{N+1} R_M}{R_R} \tag{84}$$

In the case of identical structured and sized oscillator, the nature of variations can be deemed as identical. It is ratio-metric feature and in same chip, oscillator's temperature, voltage and process variation is roughly same. The variations of measurement and reference oscillator are canceled each other. Therefore, this measurement principle makes the measurement system insensitive to PVT variation.

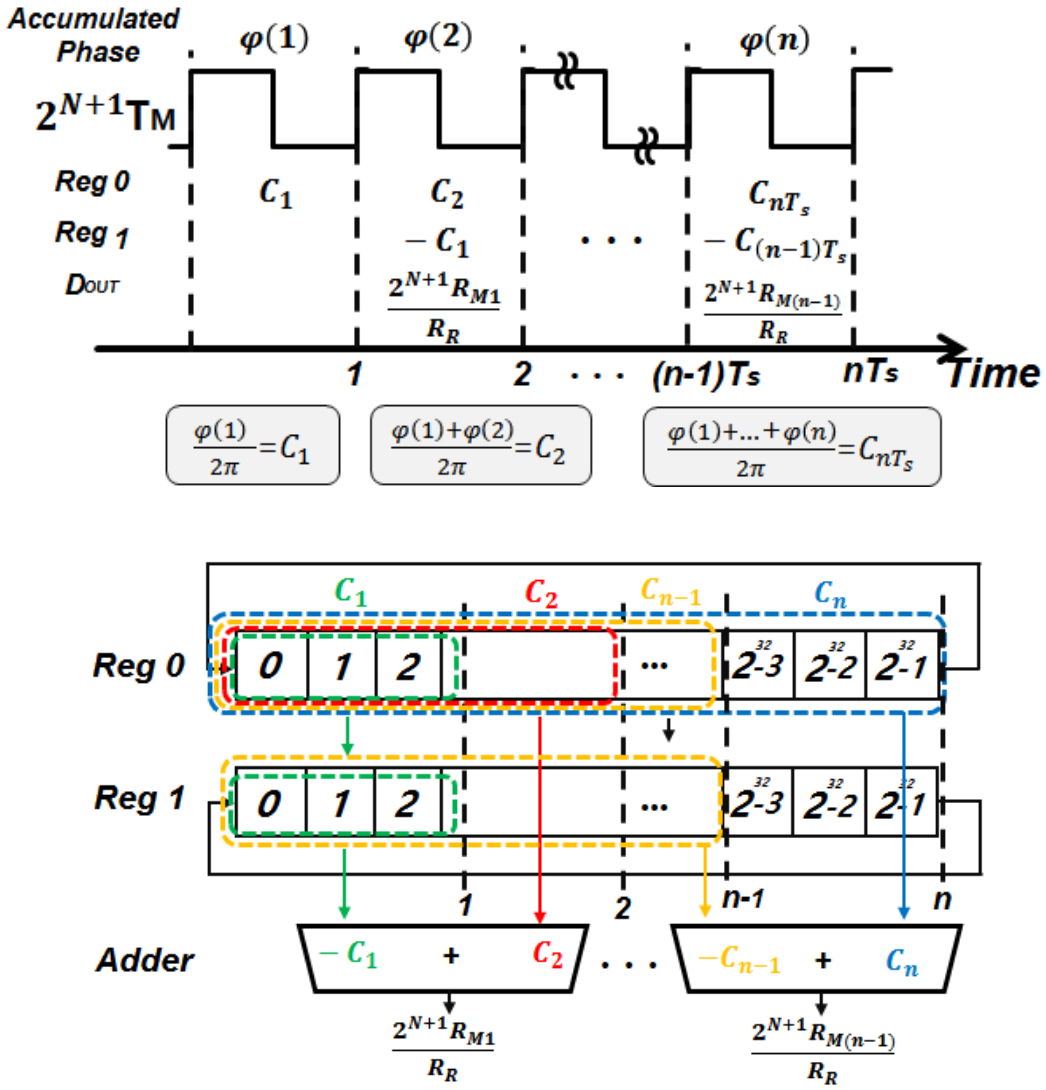

Figure 31: Timing diagram and Digital output calculation

Measured ratio is saved to Reg0 during a single cycle as shown picture and previously saved Reg1 is sent once new value is entered to next cycle. Reg1 output enters to adder as input signal reversed and resistance can be measured within one cycle.

4.4 Sensing Resolution and Trade-off with Measurement Time

The relationship between measurement time and resolution can be induced as the final digital output formula, which passed through above-obtained adder.

$$D_{OUT} = \frac{2^{N+1}\Delta R_M}{R_R} \tag{85}$$

Above formula can be rewritten as resistivity of measurement as below;

$$\Delta R_M = \frac{R_R}{2^{N+1}} D_{OUT} \tag{86}$$

Measurement resolution can be adjusted by scale factor N. In other words, resolution is increased in the case of measurement time increase. The minimum achievable value can be derived like this:

$$\varphi_{unit}(n) + 2\pi = 2\pi \left(\frac{2^{N+1}(R_M + \Delta R_{min})}{R_R}\right) \tag{87}$$

The minimum achievable resistance value is determined by the minimum time that counter counts once. Only unit phase, 2π can be counted, the faction of phase, less than 2π, can't be counted. So, this equation is expressed as the resistance resolution, ΔR_{min}.

$$\Delta R_{min} = \frac{R_R}{2^{N+1}} \tag{88}$$

5. Schematic design and Layout

In this chapter, the schematic design and layout of system circuit are introduced. First, two oscillators, measurement oscillator and reference oscillator are illustrated. Second, frequency-to-digital converter, consisting programmable frequency divider, counter, registers, and adder, is illustrated. The schematic is designed by Cadence Virtuoso Schematic Editor L and then, layout is designed by Cadence Virtuoso Layout Suite L.

5.1 Schematic design

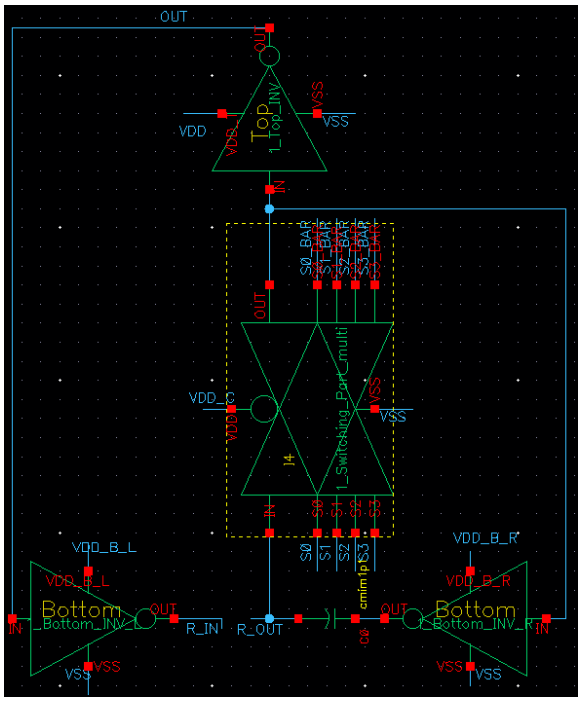

Figure 32: Schematic of measurement oscillator

Figure 32 is the schematic of measurement oscillator. It is consisted of scalable inverter, three inverters for changing the charging and discharging phase, and internal capacitor. Measurement oscillator has four switch ports for adjusting the operating number of unit inverter. There is no internal resistance. Gas sensor plays a role as the external resistance and changes the period.

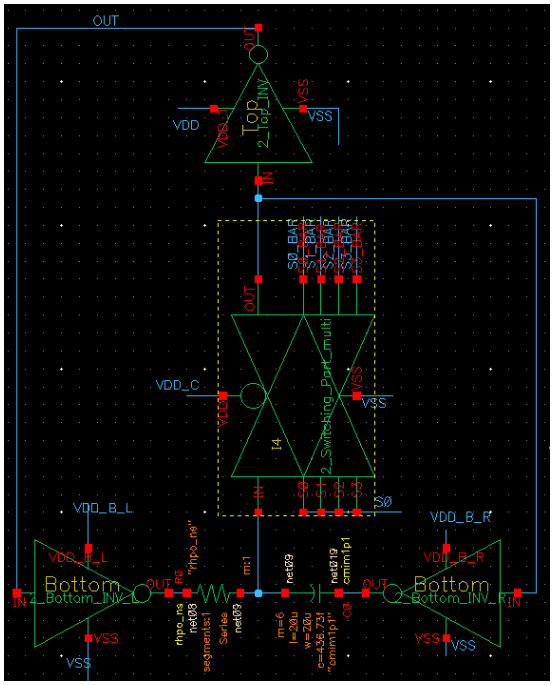

Figure 33: Schematic of reference oscillator

Figure 33 is the schematic of reference oscillator. There are two differences with measurement oscillator. There is no switch port. Oscillator works for fixed size. Reference oscillator has an internal resistance and makes constant reference period. It is generating the constant oscillation frequency.

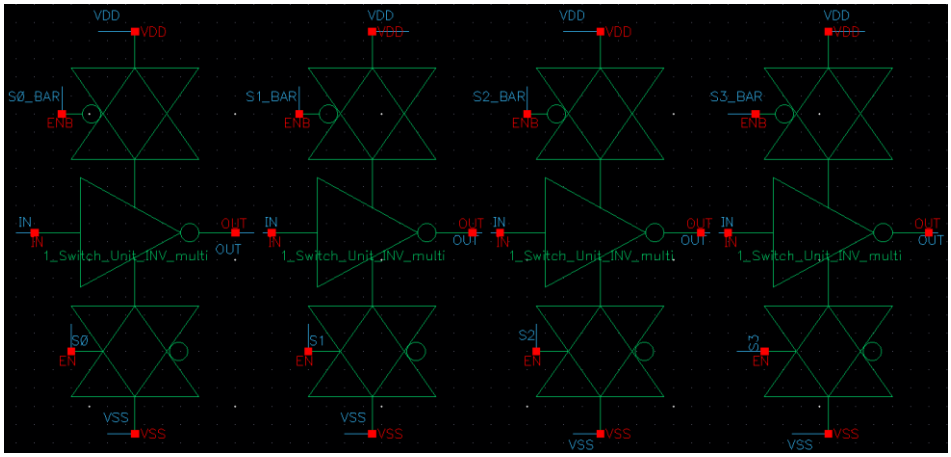

Figure 34: Scalable inverters

Figure 34 is the schematic of scalable inverters. It is consisted of transmission gates, and unit inverter. When turning on the switch, equivalent inverter size is changed. Then, power consumption and noise characteristic is changed.

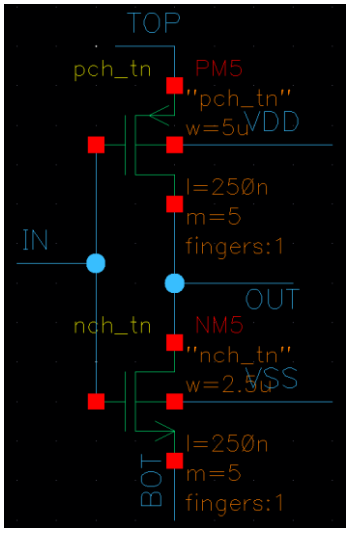

Figure 35: Unit size scalable inverter

Figure 35 is the width and length of the unit size scalable inverter. These parameters are decided for achieving optimization. To determine the size, we need to recall the FOM in chapter 2.

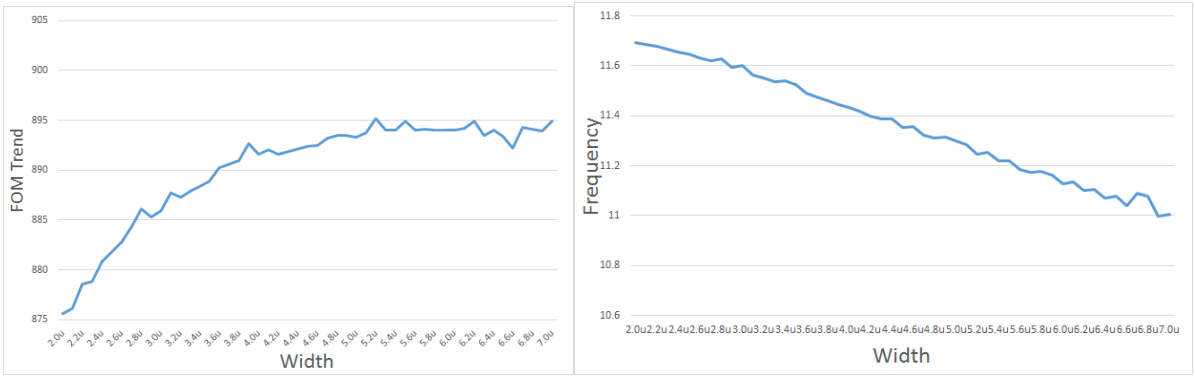

Figure 36: Relationship between FOM and width, frequency and width

Figure 36 is the relationship between FOM and inverter size (width), frequency and inverter size (width). The left side of figure illustrates that when the size of width is increased FOM also is increased. But roughly over 5 μm, FOM increment is limited. X-axis unit is μm and Y-axis is the sum of FOM from 10Hz to 1MHz. The FOM is including phase noise information according to frequency offset from center frequency and power consumption. The inverter size of width influences phase noise, center freqeuncy, and power consumption. So that, the sum of FOM at all frequency is good index for choosing the size. The right side of figure illustrates that when the size of width is increased, the clock frequency is decreased. So, the size of width can't be increased too much. In this case, the width of unit inverter of scalable inverter is choosed as 5μm.

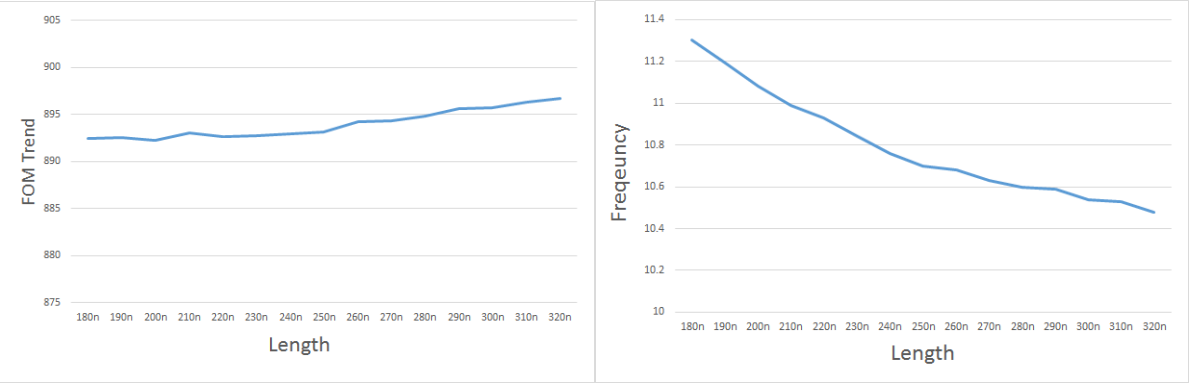

Figure 37: Relationship between FOM and length, frequency and length

Figure 37 is the relationship between FOM and inverter size (length), frequency and inverter size (length). The left side of figure ilustrates that when the size of width is increased FOM increase slightly. It is increased only several points. The variation slope is quite flat. The right side of figure illustrates the decrease of frequency. so, the size of length is suitable as much as increased length doesn't affect the frequency decrement. In this case, the length of unit inverter of scalable inverter is choosed as 0.25μm.

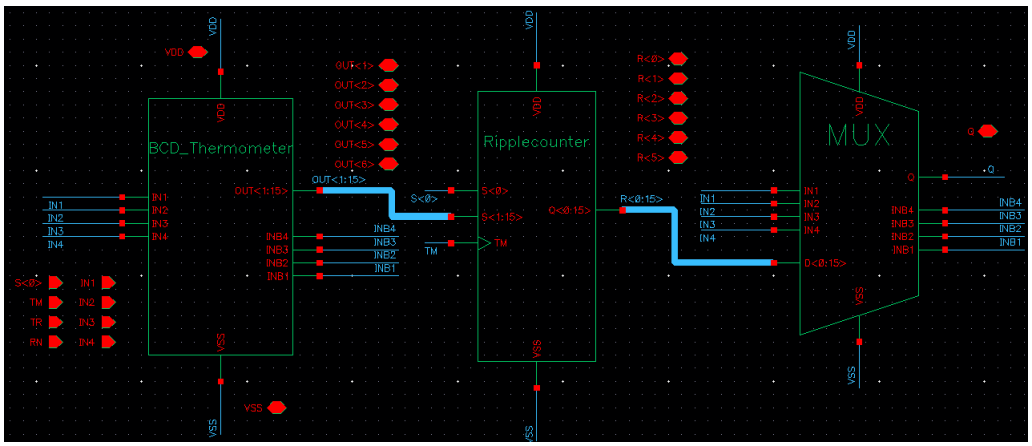

Figure 38: Programmable frequency divider

Figure 38 is programmable frequency divider. It is consisted of binary-to-decimal converter, thermometer encoder, ripple counter, and multiplexer. The binary scale factor controls the measurement window length. There are external output ports for checking the operation.

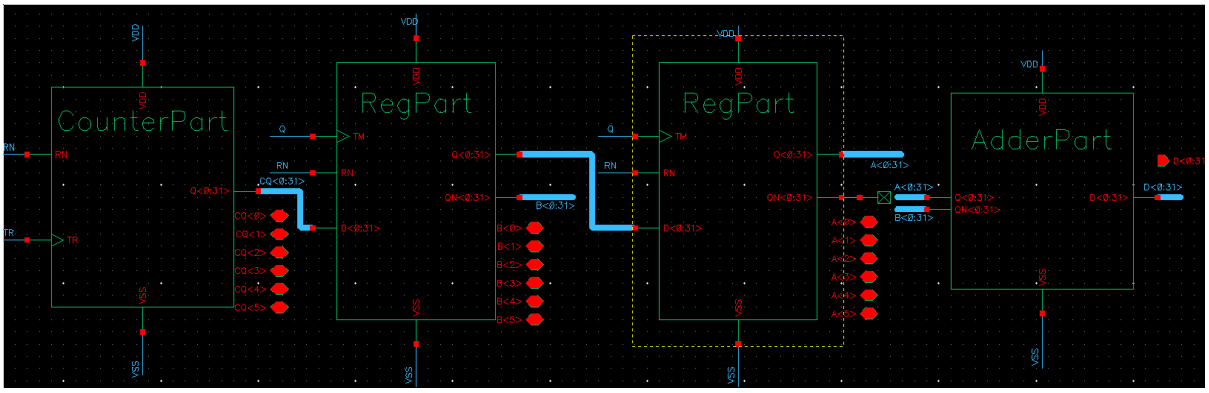

Figure 39: Counter, registers, adder

Figure 39 is digital block consisted of the counter, register, and adder. This part is counting the reference oscillation frequency within the measurement period. There are external output ports for checking the operation. There are 32 digital output ports.

5.2 Layout

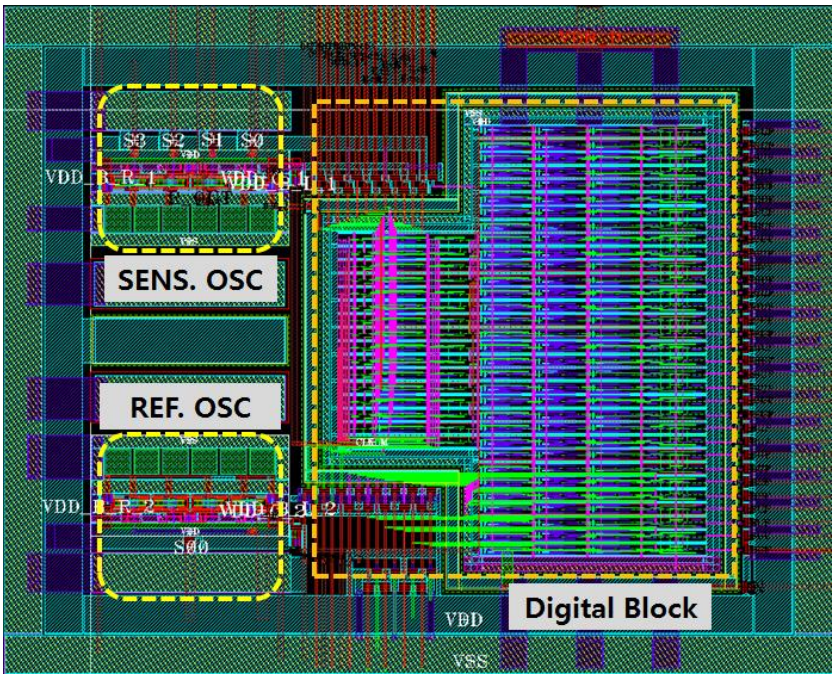

Figure 40: Top merge layout of oscillators and digital block

Figure 40 is an illustration that is top merge layout. There are oscillators and digital block. Layout details are followed below. This chip is made by Hynix/Dongbu HiTek 0.18 process applied through IDEC MPW. The system area is 660μm by 530μm.

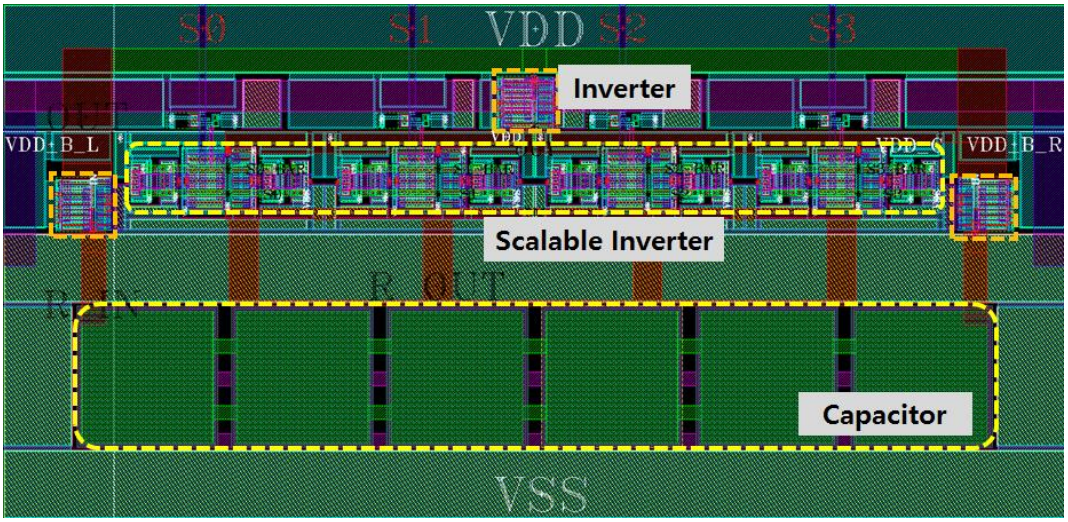

Figure 41: Layout of measurement oscillator

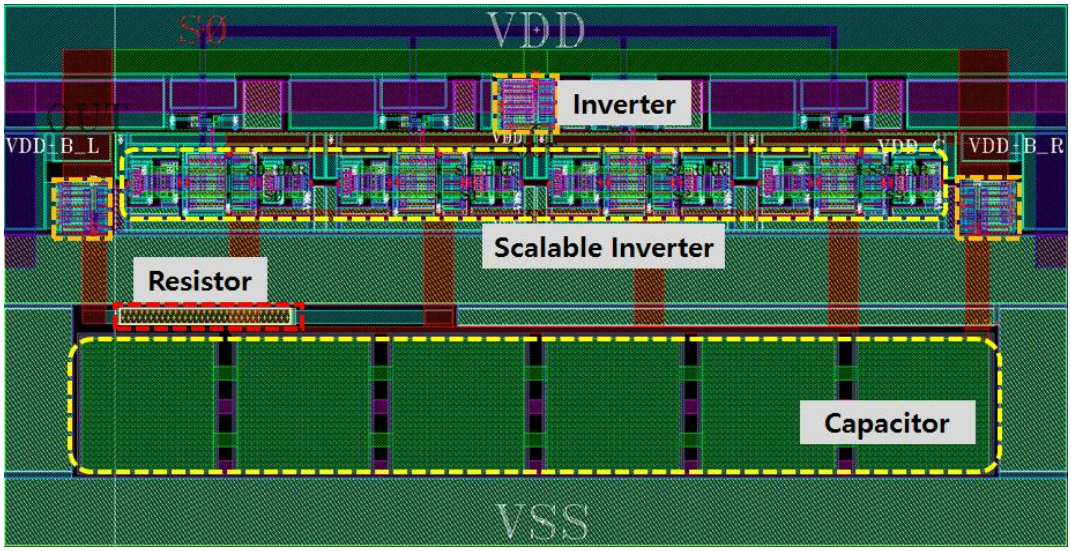

Figure 42: Layout of reference oscillator

Figure 41 and Figure 42 are two oscillators. Most of components are same each other. The size of components is equal. The difference things are that the resistor exist in reference oscillator and scale control port in measurement oscillator. The layouts have the same arrangement of elements to each other as much as possible to undergo the same process variation with each other.

Figure 43 is digital block including PDF, frequency-to-digital converter. PFD controls the length of oscillation period. Data movement direction is from left to right side. D-flip-flops are stacked in counter, registers. Digital output is coming from the right side of adder.

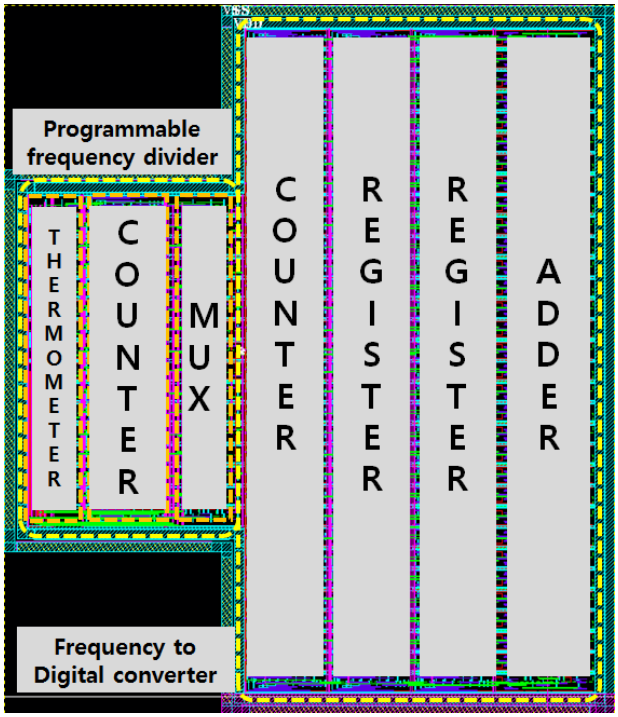

Figure 43: Digital block including PFD, Frequency-to-digital converter

6. Simulation results

In this chapter, system simulation results are introduced. Schematic simulation and post layout simulation will be verified. We will check the simulation of oscillator and digital block.

6.1 Post Layout Simulation: Oscillator

Schematic

Hz	P-noise	POWER	Frequency	FOM
10	4.145	72.45uW	11.19Mhz	128.235754
100	-25.424			137.804754
1K	-54.85			147.230754
10K	-83.641			156.021754
100K	-109.608			161.988754
1M	-131.529			163.909754
10M	-146.067			158.447754

PEX

Hz	P-noise	POWER	Frequency	FOM
10	4.647	73.89uW	11.08Mhz	127.559585
100	-24.861			137.067585
1K	-54.268			146.474585
10K	-83.206			155.412585
100K	-109.803			162.009585
1M	-132.235			164.441585
10M	-147.98			160.186585

Figure 44: Simulation results of schematic and PEX

PEX is the parasitic extraction and simulation. PEX is included the parasitic effects came from the layout result. It is more precise and similar to real performance. In Figure 44, PEX simulation results about reference oscillator are similar each other.

6.2 Post Layout Simulation: Programmable frequency converter and Frequency-to-Digital Converter

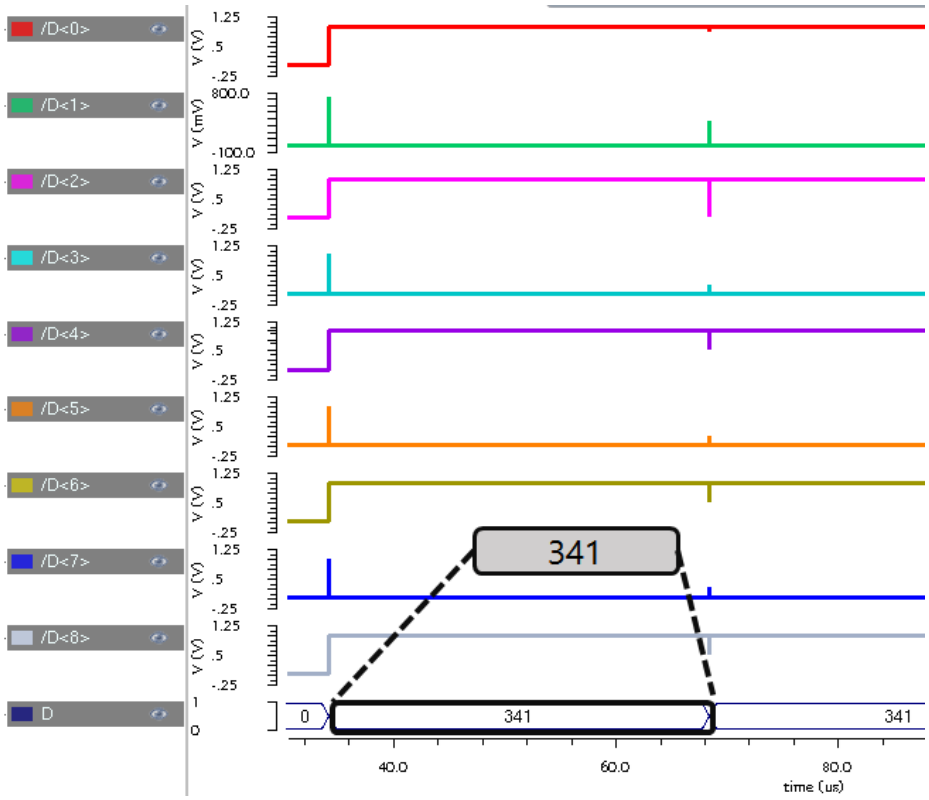

Figure 45: Simulation result of digital block

Figure 45 is the simulation result of digital block. The test setup is that the measurement frequency is 15MHz and the reference frequency is 10MHz. The capacitance value is same each other. The dividing factor N is 8. It is similar status like the measurement resistance is 10K ohm and the reference resistance is 14K ohm. In this case, we can predict the digital output value that can be calculated by using equation (83). These frequencies should be transformed as the period to measure the number of counting within the one measurement window.

$$D_{OUT} = \frac{2^{N+1}T_M}{T_R}\ , \quad D_{OUT} = \frac{2^9(66.66..nS)}{(100ns)} = \frac{512 \cdot 2}{3} \approx 341.333\ldots$$

$$R_M = \frac{D_{OUT} \cdot R_R}{2^{N+1}} = \frac{341 \cdot 14.74K}{2^9} = \frac{341}{512} \cdot 14.74K \approx 9.817\text{K}\Omega \text{ (Measured)},\ R_M = 9.712\text{K}\boldsymbol{\Omega} \text{ (simulation setup value)}$$

We can check that digital block is operating like what we expect.

6.3 Size optimization of scalable inverter based oscillator

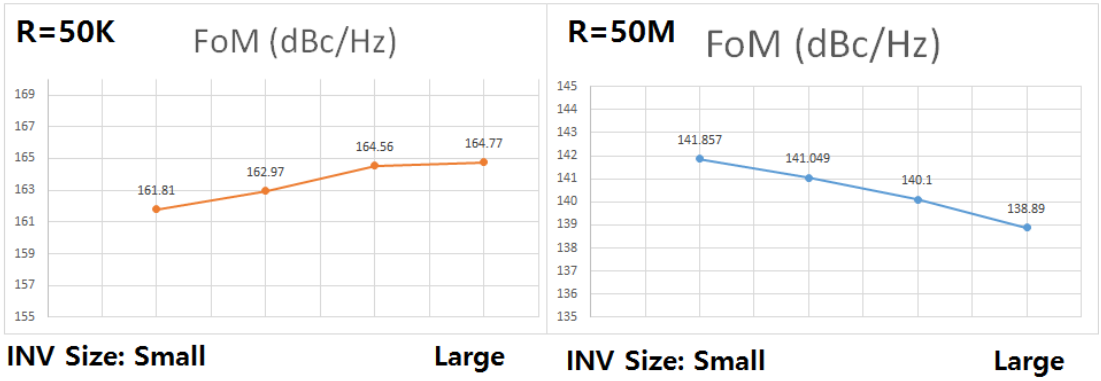

Figure 46: Figure-of-merit according to inverter size variation

Figure 46 is the result of size optimization according to resistance variation. At low resistance, oscillator makes high oscillation frequency and phase noise characteristic is more dominant than the other factor like power consumption and oscillation frequency. In other words, power consumption is slightly larger than small size, but phase noise characteristic is much better than small size. Therefore, large size is more suitable in low resistance case. At high resistance, small size of inverter is optimized. Phase noise characteristic is slightly poor than large size. However, power consumption is much less. As a result, scalable inverter based oscillator can achieve size optimization for all operation frequencies.

7. Conclusion & Future work

This thesis is started for designing gas sensor read-out circuit that has a high compatibility for large resistance measurement ranges. To achieve large-dynamic measurement range, read-out system uses RP-FDC method and it enables to adjust resolution in accordance with related purpose, using frequency divider. To achieve low power operation and high FOM, scalable inverter is proposed. In chapter 6, we verified the performance optimization of scalable inverter based oscillator. For getting better noise characteristic, swing-boosting method is accepted. The features that can obtain the large-dynamic measurement range and optimization depending to resistance change are important points for this application, gas sensor read-out circuit.

Table 10 is the comparison table about circuit performance. This circuit is designed for detecting various gases. For that purpose, large dynamic range to cover the most of commercial sensors is demanded. For the same reason, for handling the gas intensity information, frequency domain operation is better than voltage domain. Because commercial sensor's operation voltage is higher than system supply voltage. Finally, this system has the measurement range from 10K ~ 50M ohm that can measure the most of commercial gas sensors. Depending on the user's demands, measurement time can be adjusted. The resolution also can be adjustable. For any purpose, this circuit can be applied and optimized.

Parameter	**ISCAS 2011** [12]	**JSSC 2009** [23]	**JSSC 2007** [24]	**ISCAS 2007** [14]	**This work**
Technology	0.5μm	0.18μm	0.35μm	0.13μm	0.18μm
Chip Area	4.84mm^2	0.7mm^2	3.1mm^2	4.2mm^2	0.35mm^2
Method	RV-ADC	RV-ADC	RV-ADC	RP-FDC	RP-FDC
Supply voltage	3.3V	1.2V/0.5V	3.3V	1.2V	1V
Power Consumption	66μW	32μW	6mW	366μW	150μW (full load)
Measurement range	60K~10M	10K~9M	100~20M	150~85M	10K ~ 50M ohm
Measurement time	-	0.54ms	1ms	1ms	Adjustable (130ns@10K ohm, N=1 ~ 21s@50M, N=15)
Resolution	10bit	10~12bit	13bit	16bit	16 bit (Adjustable)

Table 10: Comparison table about circuit performance

Future work is to make the auto-scaling block. That is automatically control the number of turned on unit size inverter. In this thesis, the specific frequency that turns on the unit size inverter is not optimized. It need to be calibrated depending on the resistance variation. After the additional study, we can design improved circuit system that can control the inverter size depending on gas sensor resistance itself.

8. Reference

[1] 환경부, "주택 실내공기질 관리를 위한 매뉴얼," 환경부, 2012.

[2] 일. 후생노동성, "http://www.mhlw.go.jp".

[3] H. Canada, "http://www.hc_sc.gc.ca".

[4] 환경부, "실내공기질 관리 기본계획(2015~2019)," 환경부, 2015.

[5] S. H. ,. C. W. ,. D. K. a. M. T. Thorsten Wagner, "Mesoporous materials as gas sensors," *Royal society of chemistry,* no. 42, pp. 4036-4053, 2013.

[6] D. M. Wilson, S. Hoyt, J. Janata, K. Booksh and L. Obando, " "Chemical Sensors for Portable, Handheld Field Instruments"," *IEEE Sensors Journal,* p. 256–274, 2001.

[7] S. Sensortech, "MICS-4514," "https://sgx.cdistore.com/ProductDetail/MICS4514-SGX-Sensortech-Limited-formerly-e2v/333417/".

[8] AS-MLC, "AppliedSensor," "http://www.gassensor.ru/data/files/carbon_monoxide/CO_AK01.pdf".

[9] AS-MLN, "AppliedSensor," "http://www.eitlaser.com/images/No2%20gas%20sensor%20specification.pdf".

[10] AS-MLV, "AppliedSensor," "http://ams.com/eng/content/download/686543/1787717/348218".

[11] GSBT11, "Ogam," "http://d.ogamtech.com/upload/GSBT11_Ec.pdf".

[12] D. R. A. J. M. Xiaoyi Mu, ""125ppm Resolution and 120dB Dynamic Range Nanoparticle Chemiresistor Array Readout Circuit"," *IEEE International Symposium of Circuits and Systems (ISCAS) ,* pp. 2213 - 2216, 2011.

[13] M. Malfatti, M. Perenzoni, N. Viarani, A. Simoni, L. Lorenzelli and A. Baschirotto, ""A complete front-end system read-out and temperature control for resistive gas sensor array "," *Proceedings of the 2005 European Conference on Circuit Theory and Design,* vol. III, no. 3, pp. 31-34, 2005.

[14] B. Jayaraman and N. Bhat, ""High Precision 16-bit Readout Gas Sensor Interface in 0.13μm

CMOS"," *IEEE International Symposium on Circuits and Systems ,* pp. 3071 - 3074, 2007.

[15] I. S. C. C. 27, "IEEE Standard Definitions of Physical Quantities for Fundamental Frequency and Time Metrology-Random Instabilities," *IEEE std,* 2008.

[16] B. Razavi, "Design of analog CMOS integrated circuits", The McGraw-Hill Companies, Inc, 2012.

[17] J. Rutman, ""Characterization of Phase and Frequency Instabilities in Precision Frequency Sources : Fifteen Years of Progress"," *Proceedings of the IEEE,* vol. Vol. 66, no. No. 9, pp. 1048 - 1076, 1978.

[18] D. Leeso, ""A Simple Model of Feedback Oscillator Noise Spectrum"," *Proceedings of the IEEE,* vol. Vol. 54, pp. 329-330, 1966.

[19] N. Wiener, ""Generalized Harmonic Analysis"," *Acta Mathematica,* vol. Vol. 55, no. Issue 1, pp. 117-258, 1930.

[20] B. Razavi, "RF microelectronics", Prentice Hall, 2011.

[21] G. Li and E. Afshari, ""A Low-Phase-Noise Multi-Phase Oscillator Based on Left-Handed LC-Ring"," *IEEE JOURNAL OF SOLID-STATE CIRCUITS,* vol. Vol.45, no. Issue: 9, pp. 1822-1833, 2010.

[22] J. V. J. C. L. C. L. M. W. R. S. S. C. F. W. J. W. E.S. Ferre-Pikal, ""Draft Revision of IEEE STD 1139-1988 Standard Definitions of Physical Quantities for Fundamental Frequency and Time Metrology – Random Instabilities"," *IEEE International Frequency Control,* pp. 338-357, 1997.

[23] K.-J. L. J. K. A. P. C. Taeg Sang Cho, "A 32-uW 1.83-kS/s Carbon Nanotube Chemical Sensor System," *A 32-uW 1.83-kS/s Carbon Nanotube Chemical Sensor System,* vol. 44, no. 2, pp. 659 - 669 , 2009.

[24] M. Grassi, P. Malcovati and A. Baschirotto, ""A 160dB equivalent dynamic range auto-scaling interface for resistive gas sensors arrays"," *IEEE Journal of Solid-State Circuits ,* vol. 42, no. 3, pp. 518 - 528, 2007.

[25] A. K. Fung, ""A note on the Wiener-Khintchine theorem for autocorrelation "," *Proceedings of the IEEE ,* vol. Vol. 55, no. 4, pp. 594-595, 1967.